

Review

# Progress and Perspectives in the Development of Inorganic-Carbonate Dual-Phase Membrane for CO<sub>2</sub> Separation

Liyin Fu <sup>1,2</sup>, Xiaojie Shi <sup>1,2</sup>, Huiling Wu <sup>1,2</sup>, Yabin Ma <sup>1,2</sup>, Xuechao Hu <sup>3</sup> and Tianjia Chen <sup>1,2,\*</sup> 

<sup>1</sup> Chemical Engineering College, Inner Mongolia University of Technology, Hohhot 010051, China; 20221800145@imut.edu.cn (L.F.); 20221800146@imut.edu.cn (X.S.); 20231100144@imut.edu.cn (H.W.); 20231100184@imut.edu.cn (Y.M.)

<sup>2</sup> Key Laboratory of Resource Circulation at Universities of Inner Mongolia Autonomous Region, Hohhot 010051, China

<sup>3</sup> Inner Mongolia Power (Group) Co., Ltd., Inner Mongolia Power Research Institute Branch, Inner Mongolia Autonomous Region, Hohhot 010020, China; huxuechao777@126.com

\* Correspondence: tjchen@imut.edu.cn

**Abstract:** The inorganic-carbonate dual-phase membrane represents a class of dense membranes that are fabricated using diverse support materials, ranging from metals to ceramics. This dual-phase membrane consists of a porous metal or ceramic support with an introduced carbonate phase within the support pores. Compared with polymer and zeolite membranes, inorganic-carbonate dual-phase membranes exhibit exceptional CO<sub>2</sub> selectivity at elevated temperatures (>500 °C), making them an ideal choice for high-temperature CO<sub>2</sub> separation in power plant systems. The present paper provides a comprehensive overview of the separation principle, significant models, and preparation techniques employed in carbonate dual-phase membranes for CO<sub>2</sub> separation. The present study aims to discuss key factors that limit the CO<sub>2</sub> permeation performance and stability of membranes, while also exploring the potential applications of dual-phase membranes in various fields. The identification of key challenges in the future development of the carbonate dual-phase membrane has been highlighted in this work. The future trajectory of research and development should be directed toward overcoming these challenges, encompassing the synthesis technology of membranes, balance optimization of membrane structure and performance, modification of physical and chemical properties of molten carbonate, and advancement in high-temperature sealing techniques, as well as exploration of diverse membrane reactors based on carbonate dual-phase membranes for prospective applications.

**Keywords:** inorganic membrane; CO<sub>2</sub> separation; membrane reactor; high-temperature separation



**Citation:** Fu, L.; Shi, X.; Wu, H.; Ma, Y.; Hu, X.; Chen, T. Progress and Perspectives in the Development of Inorganic-Carbonate Dual-Phase Membrane for CO<sub>2</sub> Separation. *Processes* **2024**, *12*, 240. <https://doi.org/10.3390/pr12020240>

Academic Editor: Fausto Gallucci

Received: 8 December 2023

Revised: 17 January 2024

Accepted: 20 January 2024

Published: 23 January 2024



**Copyright:** © 2024 by the authors. Licensee MDPI, Basel, Switzerland. This article is an open access article distributed under the terms and conditions of the Creative Commons Attribution (CC BY) license (<https://creativecommons.org/licenses/by/4.0/>).

## 1. Introduction

The warming effects of CO<sub>2</sub> as a greenhouse gas have long been recognized. Consequently, the mitigation of CO<sub>2</sub> emissions resulting from the combustion of fossil fuels has emerged as a prominent subject in scientific research and a pressing political concern in recent years. The separation of CO<sub>2</sub> from an off-gas stream generated during industrial processes represents the primary and pivotal step for the whole CO<sub>2</sub> capture process. In industrial processes, CO<sub>2</sub> separation is commonly achieved through the implementation of four distinct technologies: chemical absorption, adsorption, low-temperature separation, and membrane-based techniques. Chemical and physical absorption techniques represent state-of-the-art CO<sub>2</sub> capture technologies, which have been successfully implemented in commercial power plant systems [1,2]. However, the limited absorption efficiency, inadequate absorptive capacity, and high energy consumption pose significant challenges to the commercial viability of CO<sub>2</sub> separation processes. Compared with other separation means, membrane separation is a continuous, cost-effective, energy-efficient, and simple-operational technology [3,4], making it particularly suitable for CO<sub>2</sub> separation.

Most research on CO<sub>2</sub>-selective membranes has focused on polymeric or microporous zeolite membranes. According to the distinctive characteristics of various materials, CO<sub>2</sub> separation membranes can be broadly categorized into four types: polymeric membranes, inorganic membranes, mixed-matrix membranes, and other membranes. The polymeric membrane is designed based on the solution-diffusion separation mechanism for CO<sub>2</sub> separation under the driving force of the concentration gradient [5]. Compared to polymeric membranes, microporous inorganic membranes provide better separation characteristics in terms of permeability and selectivity. Crystalline (such as zeolite) and amorphous (such as silica) membranes are the main types of microporous inorganic membranes [4]. Both of them generally use different pore sizes to selectively separate gases and are more chemically and thermally stable than polymer membranes. However, both the polymer and microporous membranes are not stable at an elevated temperature (>200 °C). In comparison to these membranes, the inorganic-carbonate dual-phase membrane, one of the dense inorganic membranes, exhibits superior separation permeability, selectivity, and chemical stability at high temperatures (>500 °C) [6,7]. This membrane is composed of a molten carbonate phase that fills the pores of a porous support phase, resulting in the formation of a dense dual-phase membrane. The support materials can be chosen from either an electron-conducting metal, an oxide-ion-conducting ceramic, or a mixed-O<sup>2-</sup>-e<sup>-</sup>-conducting ceramic. According to varying support materials and corresponding separation principles, the inorganic-carbonate dual-phase can be categorized into three types: (1) mixed electron and carbonate-ion conductor (MECC); (2) mixed oxide-ion and carbonate-ion conductor (MOCC), and (3) mixed ion/electron and carbonate-ion conductor (MIEC). The driving force behind the carbonate dual-phase membrane is the gradient in the electrochemical potential of CO<sub>2</sub> and/or O<sub>2</sub> present on opposite sides of the membrane. No external electricity is required for CO<sub>2</sub> separation, resulting in cost-effective CO<sub>2</sub> capture.

The unique separation characteristics of the carbonate dual-phase membrane make it highly promising for applications in combustion processes and process intensification. The utilization of high-temperature flue gas, natural gas, or fuel gas to directly heat the carbonate dual-phase membrane for CO<sub>2</sub> separation during the combustion process, such as post- or pre-combustion, can reduce the energy penalty associated with separation. The exceptional thermal and chemical stability of the carbonate dual-phase membrane significantly contributes to the process intensification. The production of hydrogen in the pre-combustion process of IGCC necessitates a sequence of procedures, including coal gasification, carbon reforming or partial oxidation, high-temperature water–gas shift, and low-temperature water–gas processing. By utilizing appropriate catalysts, a carbonate dual-phase membrane can effectively integrate the aforementioned two or three steps into a single chemical membrane reactor, demonstrating its potential as an efficient and sustainable technology. This membrane reactor, similar to most oxygen-permeable ceramic membrane reactors, exhibits a distinct permeation characteristic [6–9]. It integrates separation and reactions by effectively regulating the introduction of reactants or removal of products, thereby enhancing reactant conversion and/or product selectivity.

Previous studies have primarily focused on comparing the performance of polymer membranes and inorganic membranes for molecular separation, such as notable works by Yeong et al. [5], Lin [4], and Way [10]. Therefore, in the present review, we hope to provide comprehensive insights into the utilization of inorganic-carbonate dual-phase membranes exclusively for CO<sub>2</sub> separation. The inorganic-carbonate dual-phase membrane has been extensively investigated for approximately two decades, with a specific emphasis on enhancing its performance and durability. The advancement of such membranes relies on the exploration of appropriate materials, synthesis techniques, and structural optimization to enhance permeation performance and stability. These ongoing research and development efforts have meticulously investigated various potential industrial applications for CO<sub>2</sub> separation using membranes or membrane reactors, thereby enhancing their functionality and practicality. However, despite these concerted efforts, the realization of commercial applications has been hindered by certain technical challenges. The objective of this

study is to elucidate the properties of inorganic-carbonate dual-phase membranes for CO<sub>2</sub> separation, and to comprehensively review the advancements made in this field. Furthermore, we aim to highlight the primary challenges that these dual-phase membranes must overcome for their current applications. In parallel, we proffer insights into potential research and development trajectories for carbonate dual-phase membranes in order to cater to the demands of industrial CO<sub>2</sub> separation and applications.

## 2. Theory

### 2.1. Separation Mechanism

The dense carbonate dual-phase membrane, as an emerging technology, has been undergoing a continuous process of evolution and advancement, as illustrated in Figure 1. The concept of a metal-carbonate dual-phase membrane, initially derived from the Moten Carbonate Fuel Cell (MCFC) technology, has been recently explored in the context of academic research [11–13]. As shown in Figure 1a, the MCFC demonstrates its suitability for CO<sub>2</sub> separation when the fuel (H<sub>2</sub>) is present and an external current is continuously applied. The CO<sub>2</sub> will react with O<sub>2</sub> and electrons from the cathode to form CO<sub>3</sub><sup>2−</sup>, which is then transported by the carbonate phase to pass through the MCFC. The CO<sub>3</sub><sup>2−</sup> species ultimately underwent decomposition at the anode, yielding CO<sub>2</sub>, O<sub>2</sub>, and e<sup>−</sup>. The flow of CO<sub>2</sub> across the MCFC is determined by external currents. However, a primary drawback of MCFC for CO<sub>2</sub> separation is the low voltages permitted to prevent decomposition of the molten carbonate electrolyte. In this manner, a substantial number of stacks are required to achieve elevated currents and, accordingly, a considerable CO<sub>2</sub> capture capacity. However, this significantly escalates the cost.

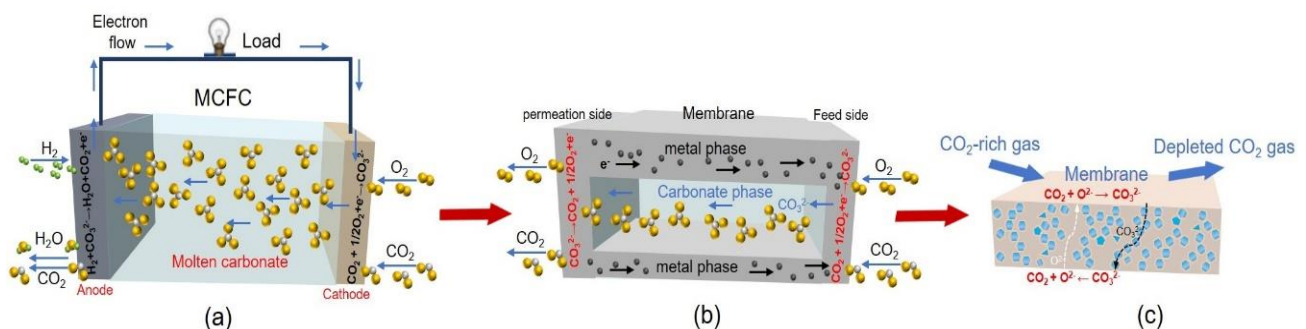


**Figure 1.** Development process of the inorganic-carbonate dual-phase membrane: (a) MCFC technology; (b) metal-carbonate dual-phase membrane; (c) dense inorganic-carbonate dual-phase membrane.

Lin and colleagues built upon the MCFC to develop a metal-carbonate dual-phase membrane for efficient CO<sub>2</sub> separation [14]. As illustrated in Figure 1b, the external circulation of the MCFC is transformed into an internal cycle of the dual-phase membrane by means of incorporating two electric conductors (metal and molten carbonate phase). The metal phase serves as a substitute for the external circuit, facilitating the electron supply for the CO<sub>3</sub><sup>2−</sup> formation reaction at the feed side ( $\text{CO}_2 + 1/2\text{O}_2 + 2\text{e}^- \rightarrow \text{CO}_3^{2-}$ ). Molten carbonates are infiltrated into the porous metal support to create a CO<sub>3</sub><sup>2−</sup> transport channel. Similarly, the generated CO<sub>3</sub><sup>2−</sup> ions will undergo decomposition into CO<sub>2</sub>, O<sub>2</sub>, and e<sup>−</sup> after traversing the membrane ( $\text{CO}_3^{2-} \rightarrow \text{CO}_2 + 1/2\text{O}_2 + 2\text{e}^-$ ). The propulsion of this process stems from the CO<sub>2</sub> pressure differential between the feed side and the permeation side, as well as the opposing transport directions of the CO<sub>3</sub><sup>2−</sup> and e<sup>−</sup> to maintain the internal electrochemical equilibrium of the membrane at elevated temperatures. Nevertheless, certain inherent limitations, as discussed in the following section, have curtailed further developments and applications of the metal-carbonate dual-phase membrane. And thus, a preferred dual-phase carbonate membrane is developed. Anderson and Lin employed a ceramic phase rather than a metal phase for the synthesis of a dense inorganic-carbonate dual-phase membrane [6]. The reaction between O<sup>2−</sup> within

the support (ceramic phase) and CO<sub>2</sub> in the feed stream is illustrated in Figure 1c, resulting in the formation of CO<sub>3</sub><sup>2-</sup> (CO<sub>2</sub> + O<sup>2-</sup> → CO<sub>3</sub><sup>2-</sup>). Subsequently, the migratory movement of CO<sub>3</sub><sup>2-</sup> toward the permeation side is observed within the carbonate phase. Pure CO<sub>2</sub> is released upon the arrival of formed CO<sub>3</sub><sup>2-</sup> at the permeation-side surface of the membrane (CO<sub>3</sub><sup>2-</sup> → CO<sub>2</sub> + O<sup>2-</sup>), and the charged oxygen ions remain in the solid phase to facilitate the combination of new CO<sub>2</sub> molecules. The ceramic phase is often a pure oxygen ionic conductor or a mixed oxygen ionic and electronic conductor with high ionic conductivity. For oxygen ionic conductors such as yttria-stabilized zirconia and doped bismuth oxide, the proposed mechanism of the ceramic–carbonate membrane is entirely applicable due to the elimination of electronic conductivity. However, for mixed oxygen ionic and electronic conductors, O<sub>2</sub> may permeate the ceramic–carbonate membrane under a feed stream with O<sub>2</sub> presence. The presence of e<sup>-</sup> transport in ceramics can facilitate the penetration of additional O<sub>2</sub> into the ceramic phase, as suggested by Rui et al. [15,16], through either surface reactions (1/2O<sub>2(gas)</sub> + 2e<sup>-</sup><sub>(ceramic)</sub> ↔ O<sup>2-</sup><sub>(ceramic)</sub>) or coupled transport of CO<sub>2</sub> and O<sub>2</sub>, analogous to the mechanism of metal–carbonate membranes (CO<sub>2(gas)</sub> + 1/2O<sub>2(gas)</sub> + 2e<sup>-</sup><sub>(ceramic)</sub> ↔ CO<sub>3</sub><sup>2-</sup><sub>(molten carbonate)</sub>), proposed by Tong et al. [17]. The prominence of these phenomena and mechanisms is not the primary consideration in instances of low O<sub>2</sub> feed pressure.

## 2.2. Comparison with Other Membranes

Table 1 presents different membranes' characteristics in terms of selectivity and permeability for CO<sub>2</sub> separation. As shown, the selectivity of polymeric membranes is often below 50, as determined by the solution-diffusion separation mechanism. However, the permeance of the polymer membrane is around 200–1000 GPU [18]. The permeance of the porous inorganic membrane, such as the zeolite membrane, can typically exceed 1000 GPU; however, the selectivity is only 20–50 [19]. Moreover, some mixed-matrix membranes show a high permeance (exceeding 3000 GPU), but the selectivity remains below 50 [20]. Basically, inorganic membranes have both permeance and selectivity significantly higher than that of polymer membranes. The permeance is about 5 to 10 times higher than that of polymer gas separation membranes under a fixed transmembrane pressure. According to the separation mechanism of the inorganic-carbonate dual-phase membrane, the primary advantage lies in its exceptional selectivity. As shown, the selectivity of the inorganic-carbonate dual-phase membranes can reach up to 200–300. Actually, the ideal selectivity of this type of membrane can theoretically approach 100% with an ideal sealing technology and high density of the membrane. However, considering the cost of materials and the preparation complexity, the industrial membrane separation processes for gas separation are dominated by polymer membranes. Most inorganic membranes for CO<sub>2</sub> separation are still in the research and development stage. The inorganic-carbonate dual-phase membrane is well suited for direct CO<sub>2</sub> separation at high temperatures, eliminating the need for additional processes and capabilities. However, further improvements are required to enhance its permeance and stability.

**Table 1.** The different membranes' characteristics in terms of selectivity and permeability for CO<sub>2</sub> separation.

Categories	Type of Membrane	CO <sub>2</sub> Selectivity	Feed Gas	CO <sub>2</sub> Flux	Ref.
Polymeric membrane	U-POMS-NW	41	CO <sub>2</sub> /N <sub>2</sub>	1000 (GPU)	[18]
Inorganic membrane	Y-zeolite	20	CO <sub>2</sub> /N <sub>2</sub>	>1000 (GPU)	[19]
mixed-matrix membrane	MgMOF-74	30	CO <sub>2</sub> /N <sub>2</sub>	>3000 (GPU)	[20]
Ceramic–carbonate membrane	Ceramic–carbonate dual-phase membranes	~100%	CO <sub>2</sub> /N <sub>2</sub>	~2000 GPU	[21,22]

### 2.3. Benchmarking Model

The development of permeation models for CO<sub>2</sub> separation through dual-phase carbonate membranes has been ongoing to achieve a more comprehensive understanding. The first CO<sub>2</sub>-permeation model based on the Wagner theory was introduced by Jerry Lin and colleagues to elucidate the metal–carbonate dual-phase membrane [14], as follows:

$$J_{CO_2} = -\frac{3RT}{8F^2L} \int_{P_t'}^{P_t''} \frac{\sigma_{CO_3^{2-}} - \sigma_e}{\sigma_{CO_3^{2-}} + \sigma_e} d(\ln P_t) \quad (1)$$

or

$$F_{CO_2} = \frac{9RT}{16F^2L} \sigma_{CO_3^{2-}} \left( \frac{\varepsilon}{\tau} \right) \ln \left( \frac{P_t'}{P_t''} \right) \left[ \frac{1}{P_t' - P_t''} \right] \quad (2)$$

where  $P_t$  is the total pressure (CO<sub>2</sub> and O<sub>2</sub> mixture).  $P_t'$  and  $P_t''$  are the total pressure of the feed side and permeation side, respectively.  $R$  is the ideal gas constant,  $T$  is the system temperature,  $F$  is Faraday's constant, and  $L$  is the membrane thickness.  $\sigma_{CO_3^{2-}}$  is the ionic conductivity of CO<sub>3</sub><sup>2-</sup> of molten carbonate phase and  $\sigma_e$  is e<sup>-</sup> conductivity of the metal phase.  $\varepsilon$  and  $\tau$  are the porosity and tortuosity of the support, respectively. The  $\sigma_{CO_3^{2-}}$  is generally much smaller than  $\sigma_e$ . After considering the microstructure ( $\varepsilon$  and  $\tau$ ) of the metal support and assuming a pressure-independent ionic conductivity, Equation (1) can be simplified to Equation (2). The suitability of this model is limited to metal–carbonate dual-phase membranes, owing to its simplification rooted in the fact ( $\sigma_e \gg \sigma_{CO_3^{2-}}$ ).

The rarity of the permeation model for metal–carbonate membranes is primarily attributed to the limited research and application of these membranes. By contrast, an array of optimistic models concerning the ceramic–carbonate dual-phase membrane has been proffered by researchers in recent years. Rui and Anderson initially and insightfully proposed a model [15], effectively merging the concept reported by Wade et al. [15] with a plausible explanation of the reported experimental data, to clarify the flux of CO<sub>2</sub>/O<sub>2</sub> across the ceramic–carbonate dual-phase membrane. Afterward, Zhang et al. further employed and derived this model to examine the CO<sub>2</sub> permeation across the ceramic–carbonate membrane [7]. Following the consideration of the microstructural effect examined by Ortiz-Landeros et al. [23], we present the summary model, which can be expressed in terms of CO<sub>2</sub> permeance ( $F_{CO_2}$ ) or flux ( $J_{CO_2}$ ), as outlined below:

$$F_{CO_2} = \sigma_T \frac{RT}{4F^2L} \ln \left( \frac{P_{feed,CO_2}}{P_{permeation,CO_2}} \right) \left[ \frac{1}{P_{feed,CO_2} - P_{permeation,CO_2}} \right] \quad (3)$$

or

$$J_{CO_2} = \sigma_T \frac{RT}{4F^2L} \ln \left( \frac{P_{feed,CO_2}}{P_{permeation,CO_2}} \right) \quad (4)$$

where  $\sigma_T$  is a permeance coefficient (or referred to as total conductance) defined by

$$\sigma_T = \frac{(\varepsilon/\tau)_s \sigma_i \cdot (\varepsilon/\tau)_p \sigma_c}{(\varepsilon/\tau)_s \sigma_i + (\varepsilon/\tau)_p \sigma_c} \quad (5)$$

and  $P_{feed,CO_2}$  and  $P_{permeation,CO_2}$  are the partial pressures of the CO<sub>2</sub> at the feed and permeate sides in Pa, respectively.  $\sigma_i$  and  $\sigma_c$  are the carbonate ionic and ceramic oxygen conductivity, respectively.  $\varepsilon$  and  $\tau$  denote the porosity and tortuosity of either the molten carbonate phase, which occupies the ceramic support pore ( $p$ ), or the solid ceramic phase ( $s$ ). The remaining symbols ( $R$ ,  $T$ ,  $F$ , and  $L$ ) correspond to those in Equation (2). Noteworthy, the  $\sigma_T$  encapsulates the inherent characteristics of the ceramic and carbonate phases (oxygen ionic and carbonate conductivity) as well as the porous and solid composition of the ceramic support (porosity or solid fraction in relation to tortuosity). The effective conductivities  $(\varepsilon/\tau)_s \sigma_i$  and  $(\varepsilon/\tau)_p \sigma_c$  are respectively assigned to the ceramic and carbonate phase.

Generally, the oxygen ionic conductivity of the ceramic phase ( $(\varepsilon/\tau)_s\sigma_i$ ) is significantly lower than the protonic conductivity ( $\sigma_c \gg \sigma_i$ ). As a result, the rate-limiting step of CO<sub>2</sub> permeation through the ceramic–carbonate membrane occurs primarily via O<sup>2−</sup> conduction within the ceramic phase.

However, the O<sup>2−</sup> conductivity of ionic or mixed-conducting ceramics is invariably contingent on the O<sup>2−</sup> partial pressure, while the O<sup>2−</sup> conduction within the ceramic phase dictates CO<sub>2</sub> permeation. Thus, it is imperative to take into account the correlation between the partial pressure of oxygen and CO<sub>2</sub>. The aforementioned model inadequately accounts for the pressure-dependent CO<sub>2</sub> permeation flux in ceramic–carbonate membranes, as it lacks a comparison with experimental flux data at varying CO<sub>2</sub> pressures. The dependency between the O<sup>2−</sup> conductivity and O<sup>2−</sup> partial pressure can be approximately characterized by a power function relationship. Norton et al. advanced a model based on such power function to adjust the total conductance, subsequently impacting CO<sub>2</sub> permeation [24]. The present model accounts for the partial pressure of impurity oxygen in the CO<sub>2</sub> and N<sub>2</sub> feeds, as well as the thermodynamic equilibrium relationship for the reaction (e.g., CO<sub>2</sub> = CO + 1/2O<sub>2</sub>). The enhanced model is presented as follows:

$$J_{CO_2} = \frac{\varnothing^m}{mq} \sigma_T \frac{RT}{4F^2L} \left[ P'_{CO_2}{}^n - P''_{CO_2}{}^n \right] \quad (6)$$

where  $\varnothing$  and  $q$  are constants. In case O<sub>2</sub> contains impurities such as CO<sub>2</sub> or N<sub>2</sub>,  $q = 1$ , and  $\varnothing$  can be determined by the level of oxygen impurities.  $m$  is a constant that may depend on temperature. Assuming  $\sigma_T$  is independent of CO<sub>2</sub> partial pressure, and given that  $n = mq$  and  $\sigma_T \sim (\varepsilon/\tau)_s\sigma_i$  as previously mentioned, Equation (6) can be simplified as follows:

$$J_{CO_2} = \frac{\varnothing^m RT}{4nF^2L} \left( \frac{\varepsilon}{\tau} \right)_s \sigma_i \left[ P'_{CO_2}{}^n - P''_{CO_2}{}^n \right] \quad (7)$$

The aforementioned models are founded on the supposition that the bulk diffusion exerts control over permeation or net CO<sub>2</sub> transport, which is dictated solely by the aggregate conductivity of the membrane. Thus, possible elementary steps, such as gradual CO<sub>2</sub> uptake and release between the feed and membrane surface, the combination of CO<sub>2</sub> with O<sup>2−</sup> and certain surface reactions, could potentially impede the overall transport rate. Marques and colleagues advanced a visual method, derived from electrochemical resistance perspectives, to detect potential kinetic limitations in addition to conventional transport models [25,26]. The research posits that any elementary step could potentially serve as the origin of an overvoltage, which may arise from either ohmic transport due to ambipolar conditions or non-ohmic processes related to surface/interface interactions. Accordingly, the actual CO<sub>2</sub> flux in membranes is depicted in Evans-type diagrams, which consist of plots of net thermodynamic voltages versus the effective cell current density. The findings of this analysis provide an innovative perspective to address overlooked aspects in the evaluation of membrane performance.

#### 2.4. Preparation

In general, the fabrication of a carbonate dual-phase membrane involves four stages: (1) precipitation of particle suspensions; (2) formulating particle suspensions into a membrane precursor with defined morphology (flat sheet or tube); (3) solidification of the membrane precursor is achieved through calcination treatment at high temperatures; and (4) molten carbonate infiltration. Hereinafter, the preparation of the ceramic–carbonate membrane will be exemplified to introduce the process, due to the currently limited investigation on the metal–carbonate membrane.

The types of support employed in ceramic–carbonate membranes encompass planar (or disk), tubular, and hollow-fiber configurations. A comprehensive approach for the synthesis of ceramic membrane precursors is presented in Table 2. The disk support is typically fabricated by directly compressing powders (without the need for particle suspen-

sions), enabling the investigation of certain fundamental properties of the membrane under laboratory conditions. The preparation of single or multichannel tubes can be achieved via the traditional extrusion method. The centrifugal casting method, a novel technique for tubular membrane preparation proposed by Dong et al. [27], enables the production of uniform tubes or tubes with thin coating layers, thereby eliminating the need for an additional coating step in the preparation of asymmetric membranes. Precision-engineered ceramic hollow-fiber membranes have been extensively researched and developed over the past decade and a half, primarily through the utilization of the phase inversion spinning process. This spinning technique, which has evolved from the preparation of polymeric hollow-fiber membranes, can be tailored to confer the membrane with an ultra-thin separating layer [28,29]. Given its potential practical applications, the tubular or hollow-fiber membrane will be given careful consideration for further research and utilization, primarily due to the outstanding packing density of the membrane module, as exemplified in Table 3. Although a scalable membrane area can be achieved through the design of multiple planar stacks, such configurations pose numerous engineering challenges, including high-temperature sealing, connection, and high-pressure resistance.

**Table 2.** Generalized procedure for precursor preparation of the ceramic membrane [30].

Shaping Technique	Suitable Model	Thickness/mm	Technical Advantage
Slip casting	disk, tube	Thick (uncontrol)	traditional, small pore size can be controlled
Tape casting	disk	0.25~1.25	large flat sheet production
Pressing	disk	>0.5	easy to fundamental research
Extrusion	tube	>0.5	multiple channels can be produced
Centrifugal casting	tube	>0.5	continuous operation for uniform coating layer
Spinning process	hollow-fiber	0.1~0.5	thin thickness can be prepared

The formation of the membrane support is exclusively achieved through the firing process of the ceramic precursor. The final step in the membrane preparation process involves the infiltration of molten carbonate. In this step, the molten carbonate can infiltrate into the pores of the ceramic support through either capillary driving force or capillary suction. The preheated molten carbonate can directly contact the support, resulting in the pores becoming fully saturated, as illustrated in Figure 2 (utilizing disk membrane as an example). As an indispensable component of the dual-phase membrane, the molten carbonate should ideally exhibit high ionic conductivity to enhance CO<sub>2</sub> permeance, as previously discussed in Section 2.2. Meanwhile, the mixed carbonate phase exhibits a high ionic conductivity exclusively in a liquid or melting state, generally speaking. The selection principle for the carbonate phase dictates that the mixed molten carbonate should possess a low melting point and high conductivity. As illustrated in Table 4, Li/Na/K carbonate demonstrates the lowest melting point, whereas Li/Na carbonate exhibits the highest conductivity. The two aforementioned combinations of carbonate are extensively employed in the research process to fabricate the membrane. Furthermore, Gude et al. [31] proposed the utilization of eutectic mixtures derived from the least volatile alkali carbonates and alkaline earth carbonates as an alternative for the fabrication of dual-phase membranes. Here, it is worth noting that the mixed carbonate phase should be formed as a eutectic mixture; otherwise, the melting point of the alkali-metal carbonate mixtures will be elevated as illustrated in Table 5 (take the Li/Na/K mixture as an example) [32].

**Table 3.** Packing density of different membrane modules.

Membrane	Module Packing Density/m <sup>2</sup> ·m <sup>3</sup> (a)
Ceramic disk	10–50
Ceramic single tube	30–300
Ceramic multichannel tube	300–500
Ceramic hollow-fiber	~1000 to 3000

(a) Data for ceramic membranes from refs. [4,28,33].

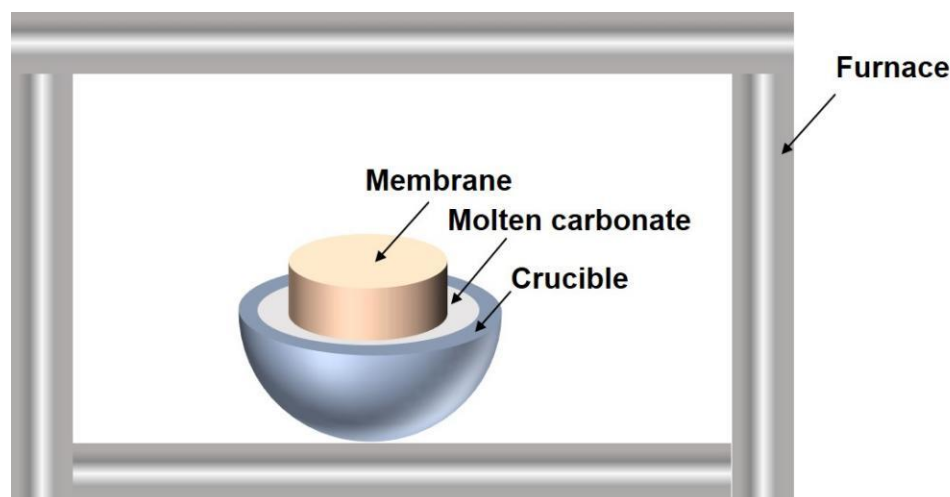


**Figure 2.** Schematic illustration of infiltration method to synthesize the dual-phase membrane.

**Table 4.** Various kinds of melting points of different carbonate mixtures for dual-phase membrane preparation [34].

Type of Mixed Carbonate	Composition/mol%	Melting Point/K	Conductivity (873/K)/S·cm	Conductivity (973/K)/S·cm
Li/Na Molten carbonate	52/48	774 <sup>(a)</sup>	1.83	2.50
Li/K Molten carbonate	62/38	761 <sup>(a)</sup>	1.15	1.65
Na/K Molten carbonate	56/44	983 <sup>(b)</sup>	1.17	1.53
Li/Na/K Molten carbonate	42.5/31.5/25	670 <sup>(a)</sup>	1.24	1.72

<sup>(a)</sup> eutectic mixture; <sup>(b)</sup> lowest melting point.

**Table 5.** Melting point of the Li/Na/K carbonate mixture with different ratios [32].

Ratio of the Li/Na/K Carbonate Mixture/mol%	Melting Point/K
43/31/25	670
0/41/59	983
0/0/100	1172
0/100/0	1131
100/0/0	999

### 3. Internal Constraints and Improvement of Membrane

The dense carbonate dual-phase membrane demonstrates promising potential for carbon capture application across various power plants, attributed to its exceptional CO<sub>2</sub> selectivity and high-temperature adaptability. The primary constraint of the carbonate dual-phase membrane for application is the restricted CO<sub>2</sub> permeation flux. The inherent properties of the membrane, such as material character and support microstructure, generally reflect intrinsic factors that contribute to its permeation performance. The primary internal determinants, consisting of porosity, tortuosity, conductivity, and thickness, define the inherent properties of the membrane, as illustrated in the aforementioned models (e.g., Equations (3)–(7)). In recent years, the development of dual-phase carbonate membranes has been focusing on overcoming their constraints to enhance CO<sub>2</sub> permeances.

### 3.1. Metal–Carbonate Dual-Phase Membrane

Regarding the metal–carbonate membrane, a significant enhancement in performance can be achieved through the optimization of support structures (i.e.,  $L$  and  $(\varepsilon/\tau)$ ). However, the impact of  $\sigma_{\text{CO}_3^{2-}}$  on the metal–carbonate membrane remains obscure, as the rate-limiting step for the permeation of the metal–carbonate membrane is  $\text{CO}_3^{2-}$  conduction within the carbonate phase, and the conductivities of various carbonate mixtures exhibit minimal discrepancies (refer to Table 4). In this context, manipulating or enhancing the  $\sigma_{\text{CO}_3^{2-}}$  component has a negligible impact on the improvement of the metal–carbonate membrane performance. The metal–carbonate membrane still exhibits notable shortcomings, in addition to the aforementioned factors: (1) The insufficient anti-oxygenation of the conventional metal, leading to a decline in  $\text{CO}_2$  permeance across the membrane at elevated temperatures. (2) The conventional metals exhibit inadequate anti-sintering and corrosion resistance capabilities (i.e., they react with molten carbonate), whereas noble metals, despite their relatively robust resistance to molten carbonate corrosion, are still cost-prohibitive. (3) The metallic support demonstrates insufficient retention capability for the liquid molten carbonate at elevated temperatures. (4) The presence of oxygen is crucial during the  $\text{CO}_2$  separation process involving metal–carbonate membranes, as previously discussed in the context of the separation mechanism, which may constrain the application scope.

Based on the intrinsic defects of the metal–carbonate membrane, Kevin Huang's group systematically optimized this type of membrane to enhance the permeation flux and stability [35–40]. To address the reaction issue between the metal and molten carbonate, Xu et al. [35] substituted stainless steel with silver as the membrane support. The Ag–carbonate membrane demonstrated a  $\text{CO}_2$  flux density of  $0.82 \text{ mL}\cdot\text{cm}^{-2}\cdot\text{min}^{-1}$  at  $650^\circ\text{C}$  with a feed gas composition of 41.67%  $\text{CO}_2$ , 41.67%  $\text{O}_2$ , and 16.66%  $\text{N}_2$  feed gas, and pure He serving as the sweep gas. The Ag support demonstrated commendable corrosion resistance. However, a comparable reduction in  $\text{CO}_2$  and  $\text{O}_2$  permeation flux above  $650^\circ\text{C}$  was also detected due to the sintering of Ag. The sintering of the porous silver support effectively “exerted pressure” on the molten carbonate at high temperature, resulting in a loss of the molten carbonate and hence a reduction in the permeation flux. Zhang et al. [37] implemented a surface coating of  $\text{Al}_2\text{O}_3$  on the porous Ag to mitigate Ag-sintering and boost the wettability between Ag and molten carbonate. The generation of  $\text{LiAlO}_2$  from the interaction between  $\text{Al}_2\text{O}_3$  and molten carbonate results in a zero-wetting angle with the molten carbonate. The findings revealed that the  $\text{Al}_2\text{O}_3$ -coated Ag–carbonate membrane could retain approximately 90% of the initial flux, whereas only approximately 15% of the original flux could be preserved for the uncoated membrane during the extended stability assessment. Tong, Fang et al. employed well-established techniques, such as chemical vapor deposition (CVD), atomic layer deposition (ALD), and chemical dealloying (CD), to achieve uniform coverage and thickness of the  $\text{Al}_2\text{O}_3$ -coated thin film, or to fabricate uniform and suitable metal structures, thereby enhancing consistency and permeation performance [39,40]. Regarding the modification and improvement of the microstructures as previously mentioned, Zhang et al. [36] also examined the influence of thickness on the permeation flux of the Ag–carbonate membrane. The critical thickness, below which the surface exchange kinetics limits the rate, for the metal–carbonate membrane was determined to be 0.84 mm. Nonetheless, despite the significant enhancements in performance and structure achieved through the aforementioned studies, the metal–carbonate dual-phase membrane does not yet constitute a prevailing research subject in this field. Integrating the working principle and inherent drawbacks of the metal–carbonate membrane, the constraints on its research and application progress are due to a “vicious circle”. The indispensable  $\text{O}_2$  in the permeation process may oxygenize or sinter the normal metal support at high temperatures, leading to a decline in permeation performance. However, despite noble metals' superior resistance to oxidation or sintering, their high cost remains a limiting factor.

### 3.2. Ceramic–Carbonate Dual-Phase Membrane

The primary distinction between the ceramic–carbonate membrane and the metal-supported membrane pertains to their overall conductivity ( $\sigma_T$ ), which is contingent on the ionic composition of the rate-limiting step. The ceramic oxygen conductivity ( $\sigma_i$ ) of the ceramic–carbonate membrane, rather than the carbonate conductivity ( $\sigma_{\text{CO}_3^{2-}}$ ), primarily determines the  $\sigma_T$  resulting from  $\sigma_e \gg \sigma_{\text{CO}_3^{2-}} \gg \sigma_i$ . Moreover, the impact of additional internal constraints ( $\epsilon$ ,  $\tau$ ,  $L$ ) on both metal and ceramic–carbonate membranes is essentially identical. Due to the unnecessary requirement of  $\text{O}_2$  in the separation process and the evident material advantages, the application scope of ceramic–carbonate membranes surpasses that of metal–carbonate membranes. And thus, the ceramic–carbonate membrane has experienced a significant acceleration in its development over the past decade. In light of internal variables, we have conducted an in-depth examination of four aspects pertaining to the ceramic–carbonate membrane: (1) unraveling the mechanism: an in-depth exploration; (2) investigation into the properties and applications of diverse ceramic materials; (3) the enhancement of preparation techniques and membrane architecture; and (4) carbonate phase reformation. For the mechanism exploration, the developments are primarily focused on the establishment of the permeation model and the working principle of the separation, which have been extensively discussed in Sections 2.1 and 2.2. These models concurrently expose the crucial internal mechanisms of the ceramic–carbonate membrane during the permeation process.

For the exploration of ceramic materials, both the chemical compatibility with carbonate and the stability of the ceramic material under high-temperature conditions should be carefully considered. In addition, the primary objective of material exploration is to promote the advancement of high-quality ceramic phases that can greatly improve oxygen ionic conductivity and subsequently enhance  $\text{CO}_2$  flux, as demonstrated in Equations (3)–(7). Generally, materials with a carbonate non-wettable property, such as those with a spinel structure, are inadequate for serving as the support material of ceramic–carbonate membranes. Various perovskite or pure ionic ceramic materials are often regarded as suitable support materials in the academic community.

The perovskite material typically exhibits a mixed ion/electron conducting (MIEC) ceramic phase. For example,  $\text{La}_{0.6}\text{Sr}_{0.4}\text{Co}_{0.8}\text{Fe}_{0.2}\text{O}_{3-\sigma}$  (LSCF), a well-known perovskite material, was first employed by Anderson and Lin for the preparation of a ceramic–carbonate membrane [6]. The porous LSCF skeleton had an average pore size of 182 nm, with  $\text{CO}_2$  permeance values of 2.01, 3.73, 4.63, and  $4.77 \times 10^{-8} \text{ mol}\cdot\text{m}^{-2}\cdot\text{s}^{-1}\cdot\text{Pa}^{-1}$  at 900 °C, corresponding to thicknesses of 3.0, 1.5, 0.75, and 0.375 mm, respectively. The  $\text{CO}_2$  flux at membrane thicknesses of 3.0 and 1.5 mm was in good agreement with the model prediction reported by Rui et al. [15], indicating that  $\text{O}^{2-}$  conduction in the LSCF phase represents the rate-limiting step. The  $\text{CO}_2$  flux in the experimental data deviated from the predicted results as the membrane thickness diminished to 0.75 and 0.375 mm, indicating the involvement of surface reaction kinetics during the permeation process. Norton et al. [41] used  $\text{La}_{0.85}\text{Ce}_{0.1}\text{Ga}_{0.3}\text{Fe}_{0.65}\text{Al}_{0.05}\text{O}_{3-\sigma}$  (LCGFA), an A-site deficient perovskite oxide, to mitigate  $\text{CO}_2$  attack on the perovskite support and boost membrane stability. The findings revealed that the  $\text{CO}_2$  flux obtained at 900 °C utilizing 50%  $\text{CO}_2$ -He as the feed gas reached  $0.024 \text{ mL}\cdot\text{cm}^{-2}\cdot\text{min}^{-1}$  (with a membrane thickness of 1.5 mm), demonstrating a stable flux between 0.021 and  $0.025 \text{ mL}\cdot\text{cm}^{-2}\cdot\text{min}^{-1}$  for a duration of 275 h at 900 °C. The  $\text{CO}_2$  flux was markedly diminished compared to that of the LSCF–carbonate membrane ( $4.63 \times 10^{-8} \text{ mol}\cdot\text{m}^{-2}\cdot\text{s}^{-1}\cdot\text{Pa}^{-1}$  versus  $\sim 0.35 \text{ mL}\cdot\text{cm}^{-2}\cdot\text{min}^{-1}$ ) under identical conditions. The main reason for the distinction is due to the much lower oxide-ion conductivity ( $\sigma_i$ ) of LCGFA ( $0.03 \text{ S}\cdot\text{cm}^{-1}$  at 900 °C) compared to that of LSCF ( $0.1 \text{ S}\cdot\text{cm}^{-1}$  at 900 °C). Lan et al. [42] fabricated a  $\text{La}_{0.5}\text{Sr}_{0.5}\text{Fe}_{0.8}\text{Cu}_{0.2}\text{O}_{3-\sigma}$  (LSFCu)–carbonate membrane using 10 wt%  $\text{LiAlO}_2$  to enhance the wettability between the molten carbonate and the support. The maximum  $\text{CO}_2$  flux of approximately  $0.55 \text{ mL}\cdot\text{cm}^{-2}\cdot\text{min}^{-1}$  was realized at 750 °C, utilizing a 50%  $\text{CO}_2$ /50%  $\text{N}_2$  gas mixture as the feedstock. Compared to the LSCF–carbonate membrane, the total conductivity ( $\sigma_T$ ) of the LSFCu support ( $70 \text{ S}\cdot\text{cm}^{-1}$  at

800 °C) demonstrates a higher value than that of the porous LSCF support ( $\sim 42 \text{ S}\cdot\text{cm}^{-1}$  at 800 °C), resulting in an elevated  $\text{CO}_2$  permeation flux.

Pure ionic conductors with excellent carbonate-wetting properties, in addition to perovskite materials, have also been examined in the development of ceramic-carbonate membranes. Wade et al. [32] employed an in situ method to synthesize 8-mol% yttria-doped zirconia (YSZ), 10-mol% gadolinia-doped ceria (CGO or GDC), and  $\alpha\text{-Al}_2\text{O}_3$ -carbonate membranes for  $\text{CO}_2$  separation. The implementation of an  $\alpha\text{-Al}_2\text{O}_3$  non-oxide conducting membrane was strategically employed to investigate the correlation between oxide ion conductivity and the underlying transport mechanism. The  $\text{CO}_2$  permeance of the  $\text{Al}_2\text{O}_3$ -carbonate membrane remained below  $2.6 \times 10^{-9} \text{ mol}\cdot\text{m}^{-2}\cdot\text{s}^{-1}\cdot\text{Pa}^{-1}$  throughout its 4000 min test at 750 °C, indicating that the insulating material or the non-oxide conducting membrane did not facilitate a  $\text{CO}_2$  flux. By contrast, the  $\text{CO}_2$  permeance of the YSZ- and CGO-based carbonate membranes stands at  $2.0 \times 10^{-8}$  and  $3 \times 10^{-8} \text{ mol}\cdot\text{m}^{-2}\cdot\text{s}^{-1}\cdot\text{Pa}^{-1}$ , respectively, at 750 °C. However, the  $\text{CO}_2$  flux does not appear to yield satisfactory results, potentially due to the limited oxygen ionic conductivity. The comparison of  $\text{O}^{2-}$ -conductivity across various ceramic supports is presented in Table 6. As illustrated, YSZ exhibits the lowest  $\text{O}^{2-}$  conductivity among all the materials investigated. Fluorite-structured  $\text{Bi}_{1.5}\text{Y}_{0.3}\text{Sm}_{0.2}\text{O}_3$  (BYS), known for its superior oxide-ion conductivity (refer to Table 6), was employed by Li et al. [43] and Rui et al. [44] for the preparation of the ceramic-carbonate membrane. A thin  $\gamma\text{-Al}_2\text{O}_3$  film was implemented to enhance the wettability between the BYS surface and carbonate phase. As anticipated, a significant increase in  $\text{CO}_2$  flux was observed compared to the YSZ-carbonate membrane [44]. The  $\text{CO}_2$  flux was  $0.083 \text{ mL}\cdot\text{cm}^{-2}\cdot\text{min}^{-1}$  at 650 °C with 50%  $\text{CO}_2$ /50% Ar and a He sweep gas flow rate of  $125 \text{ mL}\cdot\text{min}^{-1}$  (STP). Due to the significantly higher  $\text{O}^{2-}$  conductivity ( $\sigma_i$ ) exhibited by BYS, it is expected that the thin ( $\sim 50 \mu\text{m}$ ) BYS-carbonate membrane would demonstrate a  $\text{CO}_2$  flux exceeding  $0.15 \text{ mL}\cdot\text{cm}^{-2}\cdot\text{min}^{-1}$ , approximately 15 times greater than the flux ( $0.12 \times 10^{-8} \text{ mol}\cdot\text{m}^{-2}\cdot\text{s}^{-1}\cdot\text{Pa}^{-1}$  or  $0.01 \text{ mL}\cdot\text{cm}^{-2}\cdot\text{min}^{-1}$ ) of the thicker (200–400  $\mu\text{m}$ ) YSZ-carbonate membrane at 650 °C. Nonetheless, the quantified flux of the BYS-carbonate membrane exhibits merely an approximately eightfold increment compared to that of the thick membrane. The comparison implies that the ultimate performance of the membrane is also influenced by other internal factors.

**Table 6.** Comparison of the  $\text{O}^{2-}$  conductivity of different ceramic supports.

Ceramic Phase	Temperature/°C	$\sigma_i/\text{S}\cdot\text{cm}^{-1}$	Ref.
$\text{La}_{0.6}\text{Sr}_{0.4}\text{Co}_{0.8}\text{Fe}_{0.2}\text{O}_{3-\delta}$ (LSCF)	700	0.024	[6]
$\text{Y}_{0.16}\text{Zr}_{0.84}\text{O}_{2-\delta}$ (YSZ)	650	0.01	[32]
CGO or GDC	650	0.029	[32]
$\text{Bi}_{1.5}\text{Y}_{0.3}\text{Sm}_{0.2}\text{O}_{3-\delta}$ (BYS)	650	0.14	[44]
$\text{Ce}_{0.8}\text{Sm}_{0.2}\text{O}_{1.9}$ (SDC)	700	0.02	[45]

For the advancement of preparation techniques and membrane architecture, the research objectives primarily revolve around thickness ( $L$ ) and microstructures ( $\epsilon/\tau$ ), neglecting the  $\sigma_i$  of the materials (see Equations (3)–(5)). The permeation of  $\text{CO}_2$  through dual-phase membranes is governed by oxygen ionic transport; thus, the utilization of thin membranes can effectively reduce ion transport resistance by shortening the diffusion path. Thus, a significant reduction in the thickness of the dual-phase membrane represents a viable strategy for achieving elevated  $\text{CO}_2$  flux.

Lu and Lin documented a method for the fabrication of an asymmetric ceramic-carbonate dual-phase membrane [46]. The two-layer asymmetric support system consisted of a large pore base support and a thin, small pore ionic conducting ceramic top layer. The crux of this concept is to guarantee that the top layer serves as an efficient gas-tight permeable bed for  $\text{CO}_2$  separation, while the bottom layer remains porous to facilitate unobstructed gas mixture passage, as illustrated in Figure 3. The utilization of varying capillary forces generated from distinct pore sizes and wettability characteristics of carbonate

substrates was conducted to achieve this result. After conducting an in-depth investigation into various combinations of diverse materials, including YSZ, LSCF, BYS, and  $\alpha$ -Al<sub>2</sub>O<sub>3</sub>, an optimal thin YSZ top-layer/thick BYS porous layer combination was ultimately fabricated. The CO<sub>2</sub> flux of the asymmetrical YSZ/carbonate-BYS dual-phase membrane was 0.59 mL·cm<sup>-2</sup>·min<sup>-1</sup> at 650 °C, which exceeded the values of 5 to 10 times for the thicker dual-phase membranes mentioned previously. Similar to the above concept, Dong et al. [27] recently advanced a novel asymmetric tubular Ce<sub>0.8</sub>Sm<sub>0.2</sub>O<sub>1.9</sub> (SDC)–carbonate membrane. This membrane is fabricated from a thin SDC–carbonate dense layer and a porous SDC/BYS support. Since BYS is a carbonate non-wettable material mentioned above, only the porous SDC thin layer will be filled with the carbonate, hence forming a thin and dense SDC–carbonate membrane (with ~0.150 mm thickness) supported by a porous SDC/BYS matrix (with 1.35 mm thickness). The maximal CO<sub>2</sub> flux and permeance of the asymmetric tubular membrane reached 1.56 mL·cm<sup>-2</sup>·min<sup>-1</sup> and  $2.3 \times 10^{-7}$  mol·m<sup>-2</sup>·s<sup>-1</sup>·Pa<sup>-1</sup>, respectively, at a temperature of 900 °C. This membrane demonstrates a comparable separation performance to the asymmetrical YSZ/carbonate-BYS membrane reported by Lu and Lin [39], with a value of 0.44 mL·cm<sup>-2</sup>·min<sup>-1</sup> versus 0.59 mL·cm<sup>-2</sup>·min<sup>-1</sup>, under similar conditions (650~700 °C, 50% CO<sub>2</sub>/50% N<sub>2</sub> feed gas) [47].

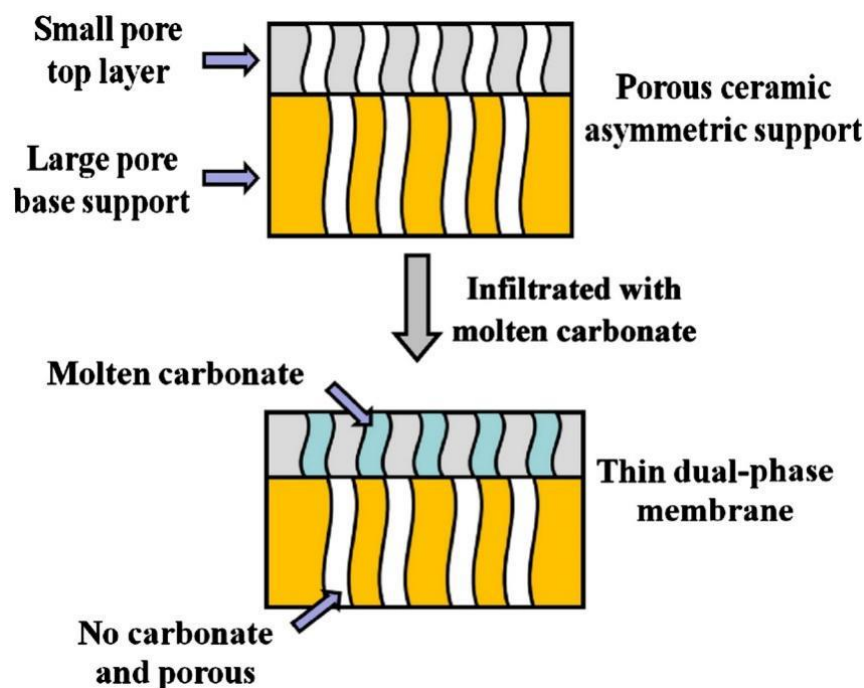


**Figure 3.** Schematic configuration of asymmetric thin dual-phase membrane (reprinted from [46] with permission of Elsevier).

In addition to the aforementioned “coating-layer” strategy, fabricating a dual-phase membrane based on hollow-fiber technology is another approach to reduce the membrane thickness. Zuo et al. conducted a pioneering study to fabricate a ceramic–carbonate hollow-fiber membrane utilizing YSZ as the supporting material [48]. The CO<sub>2</sub> flux values were 0.061 and 0.13 mL·cm<sup>-2</sup>·min<sup>-1</sup> at 650 °C and 850 °C, respectively, which were consistent with the findings reported by Wade et al. (0.047 or 0.17 mL·cm<sup>-2</sup>·min<sup>-1</sup> at 650 or 850 °C). Although the performance of the YSZ–carbonate hollow-fiber membrane might not be as optimal as expected due to its relatively thicker membrane thickness (0.3–0.5 mm), the successful preparation of such membranes in a hollow-fiber geometry nonetheless offers a novel perspective for high-temperature CO<sub>2</sub> separation using ceramic–carbonate membranes. After that, Zhuang et al. [49] synthesized a LSCF–carbonate hollow-fiber membrane with a thickness of approximately 0.3 mm. The CO<sub>2</sub> flux density can reach up to 1.0 mL·cm<sup>-2</sup>·min<sup>-1</sup> at 900 °C, which surpasses the disk-shaped LSCF–carbonate

membrane (0.375 mm thickness) reported by Anderson and Lin under the same measurement conditions ( $0.36 \text{ mL}\cdot\text{cm}^{-2}\cdot\text{min}^{-1}$  at  $900 \text{ }^\circ\text{C}$ ). Jiang et al. [50] fabricated a multichannel hollow-fiber membrane with a 0.22 mm thickness and  $\text{SrFe}_{0.8}\text{Nb}_{0.2}\text{O}_{3-\sigma}$  (SFN) as the support matrix, as illustrated in Figure 4. The peak  $\text{CO}_2$  flux value was  $0.64 \text{ mL}\cdot\text{cm}^{-2}\cdot\text{min}^{-1}$ , which was achieved using a 50%  $\text{CO}_2/50\% \text{ N}_2$  feed gas at a temperature of  $850 \text{ }^\circ\text{C}$ .

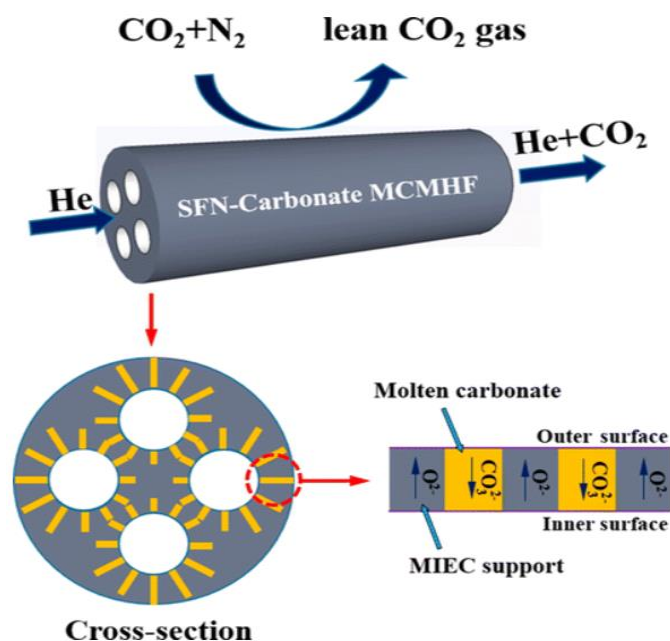


**Figure 4.** Schematic configuration of multiple channel SFN-carbonate membrane (reprinted from [50] with permission from ACS publications).

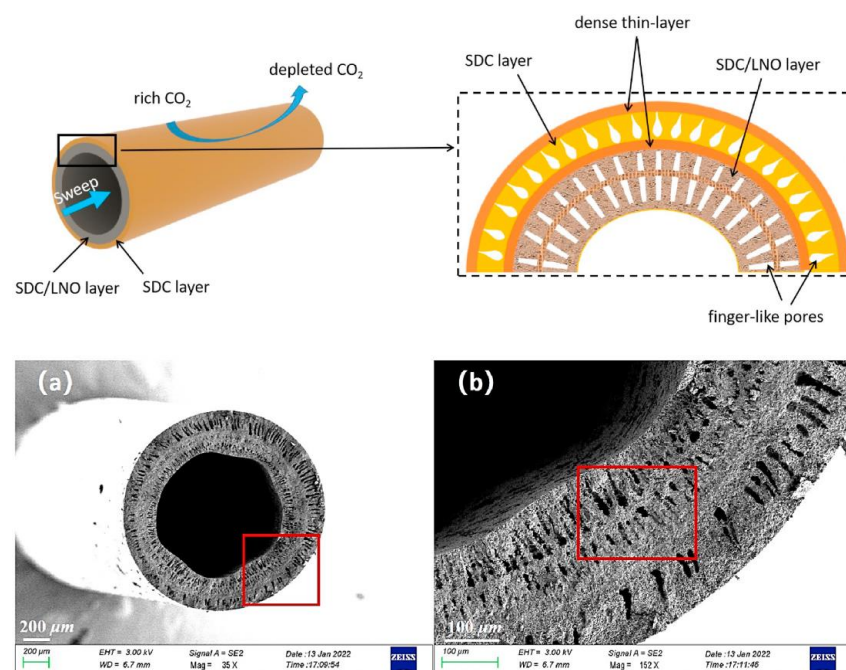
The microstructure of the dual-phase membrane is considered a crucial internal factor that determines its performance. Table 7 presents a comprehensive analysis of the impact of membrane thickness and microstructure on  $\text{CO}_2$  permeation in typical studies utilizing ceramic-carbonate dual-phase membranes, summarizing their major findings. Ortiz-Landeros et al. [23] provided a comprehensive investigation into the impact of support structures on  $\text{CO}_2$  permeance in dual-phase membranes. The findings demonstrated that an increase in the  $\text{CO}_2$  flux of dual-phase membranes can be achieved by elevating four parameters: carbonate conductivity ( $\sigma_c$ );  $\text{O}^{2-}$  conductivity for ceramic phase ( $\sigma_i$ ); the ratio of porosity (or carbonate phase) to tortuosity ( $(\varepsilon/\tau)_p$ ); and the ratio of the solid fraction to tortuosity ( $(\varepsilon/\tau)_s$ ), as depicted in Equations (4) and (5). Maximizing the total conductance ( $\sigma_T$ ) will guide the design and optimization of the ceramic matrix structure to achieve the maximum  $\text{CO}_2$  flux. As previously mentioned, for the majority of ceramic dual-phase membranes, the  $\sigma_c$  values are approaching for kinds of carbonate mixture, with  $\sigma_c \gg \sigma_i$ . Thus, besides the  $\sigma_i$  value being determined by the materials, an effective strategy to fabricate membranes with enhanced  $\text{CO}_2$  permeance is to elevate the  $(\varepsilon/\tau)_s$  term. The porous SDC support prepared by the “sacrificial-template” method, as reported by Zhang et al. [7], serves as a notable example of an approach that effectively achieves high  $\text{CO}_2$  permeance. The data presented in Table 6 demonstrate that the SDC-carbonate membrane, with a thickness of 1.2 mm, achieved a  $\text{CO}_2$  flux of  $1.84 \text{ mL}\cdot\text{cm}^{-2}\cdot\text{min}^{-1}$  under a gas mixture of 4.8%  $\text{H}_2/47.6\% \text{ CO}_2/47.6\% \text{ N}_2$  at  $700 \text{ }^\circ\text{C}$ . Although the SDC-carbonate membrane exhibits a relatively greater thickness (1.2 mm), its permeability is at least twofold higher than that reported for YSZ- and CGO-based carbonate membranes at  $650 \text{ }^\circ\text{C}$  and at least one order of magnitude greater than the LSCF-carbonate membrane at  $700 \text{ }^\circ\text{C}$ . The substantial enhancement of  $\text{CO}_2$  flux can be attributed to the efficient microstructure.

Table 7. Comparison of the results of typical studies based on the ceramic–carbonate dual-phase membrane.

Ceramic Material	Membrane Geometry	Thickness/mm	CO <sub>2</sub> Flux at Medium Temp. (for Comparison)/ mL·min <sup>-1</sup> ·cm <sup>-2</sup>	Max. CO <sub>2</sub> Flux in the Reports/mL·min <sup>-1</sup> ·cm <sup>-2</sup>	Feed Gas Composition	ε	ε/τ	Ea/kJ·mol <sup>-1</sup>	Ref.
LSCF	Disk	0.375	0.06 (700 °C)	0.36 (900 °C)	50% CO <sub>2</sub> /50% Ar	-	0.145	89.9	[6]
LSCF	Hollow-fiber	~0.3	0.31 (700 °C)	1.00 (900 °C)	50% CO <sub>2</sub> -50% N <sub>2</sub>	-	-	56.8	[49]
LSFCu	Disk	1.5	0.32 (700 °C)	0.55 (900 °C)	50% CO <sub>2</sub> /50% N <sub>2</sub>	-	-	74.3	[42]
LCGFA	Disk	0.75		0.044 (900 °C)	50% CO <sub>2</sub> /50% He	0.40	0.134	96.0	[41]
BYS	Disk	0.05	0.083 (650 °C)	0.083 (650 °C)	50% CO <sub>2</sub> /50% Ar	-	0.107	113.0	[44]
YSZ	Disk	0.2~0.4	~0.05 (650 °C)	0.17 (850 °C)	50% CO <sub>2</sub> /50% He	0.34	-	84.0 ± 14.0	[32]
YSZ/BYS	Disk	~0.01	0.59 (650 °C)	0.59 (650 °C)	25% CO <sub>2</sub> /75% N <sub>2</sub>	0.46	-	106.0	[46]
YSZ	Hollow-fiber	~0.5	0.061 (650 °C)	0.22 (950 °C)	50% CO <sub>2</sub> -50% N <sub>2</sub>	-	-	50.7	[48]
SDC/SDC-BYS	Tube	~0.15	0.44 (700 °C)	2.04 (900 °C)	50% CO <sub>2</sub> -50% N <sub>2</sub>	0.28	-	83.3	[21]
SDC/SDC-BYS	disk	~0.15	0.88 (700 °C)	0.88 (700 °C)	50% CO <sub>2</sub> -50% N <sub>2</sub>	0.35	-	-	[47]
SDC	Disk	1.2	1.84 (700 °C)	1.84 (700 °C)	4.8% H <sub>2</sub> /47.6% CO <sub>2</sub> /47.6% N <sub>2</sub>	0.53	0.234	77.2	[7]
SDC	Disk	1.5	0.31 (700 °C)	0.79 (900 °C)	50% CO/35% CO <sub>2</sub> /10% H <sub>2</sub> /5% N <sub>2</sub>	0.36	-	54.0	[24]
SDC	Hollow-fiber	0.1~0.15	4.78 (700 °C)	4.78 (700 °C)	50% CO <sub>2</sub> /50% N <sub>2</sub>	0.43	0.054	88.1	[51]
SDC	Hollow-fiber	0.1~0.15	5.46 (700 °C)	5.46 (700 °C)	5% H <sub>2</sub> /47.5% CO <sub>2</sub> /47.5% N <sub>2</sub>	0.43	0.054	85.6	[51]
LSFM <sup>a</sup>	Disk	1–2		0.211 (800 °C)	50% CO <sub>2</sub> /50% N <sub>2</sub>	-	-	88.6	[52]
LSN <sup>a</sup>	Disk	0.8	0.12 (750 °C)	1.08 (850 °C)	75% N <sub>2</sub> /15% CO <sub>2</sub> /10% O <sub>2</sub>	-	-	206.9	[53]
SFN <sup>a</sup>	Multichannel Hollow-fiber	0.22	0.31 (700 °C)	0.64 (850 °C)	50% CO <sub>2</sub> /50% N <sub>2</sub>	-	-	44.8	[50]

LSFM<sup>a</sup>: La<sub>0.2</sub>Sr<sub>0.8</sub>Fe<sub>0.9</sub>Mo<sub>0.1</sub>O<sub>3-δ</sub>; LSN<sup>a</sup>: La<sub>1.5</sub>Sr<sub>0.5</sub>NiO<sub>4±δ</sub>; SFN<sup>a</sup>: SrFe<sub>0.8</sub>Nb<sub>0.2</sub>O<sub>3-δ</sub>.

The ceramic–carbonate membrane will exhibit superior CO<sub>2</sub> permeability when it simultaneously possesses a reduced thickness and an optimized microstructure. For instance, Chen et al. [51] fabricated an SDC–carbonate hollow-fiber membrane through the application of phase inversion and spinning techniques. The SDC–carbonate hollow-fiber membrane exhibits a thickness ranging from 0.1 to 0.15 mm, attributed to its asymmetrical structure. Meanwhile, a higher degree of porosity and lower tortuosity contribute to the increased value of ( $\epsilon/\tau$ ) as demonstrated in Table 7. The membrane demonstrated exceptional CO<sub>2</sub> permeation performance under various feed conditions. At temperatures of 700 °C, the maximum CO<sub>2</sub> fluxes are 4.78, 5.46, and 1.79 mL·cm<sup>-2</sup>·min<sup>-1</sup>, respectively, under feeding conditions of 50% CO<sub>2</sub>-50% N<sub>2</sub>, 5% H<sub>2</sub>-47.5% CO<sub>2</sub>-47.5% N<sub>2</sub>, and 5% O<sub>2</sub>-20% CO<sub>2</sub>-75% N<sub>2</sub>. Compared to the work of Zhang et al. [7], the disk SDC membrane exhibits a superior microstructure, resulting in a larger ( $\epsilon/\tau$ ) value of 0.233, which is approximately four times greater than that of the SDC hollow-fiber membrane (0.0544). However, the thickness of the disk SDC membrane (1.2 mm) is approximately 10 times thicker than that of the SDC–carbonate hollow-fiber membrane (0.1–0.15 mm). As a result, the SDC–carbonate hollow-fiber membrane exhibits a superior performance under comparable test conditions (5.46 mL·cm<sup>-2</sup>·min<sup>-1</sup> versus 1.84 mL·cm<sup>-2</sup>·min<sup>-1</sup>), as illustrated in Table 7. However, the mechanical strength of this SDC–carbonate hollow membrane is significantly inadequate. Chen et al. [22] successfully enhanced the stability and mechanical robustness of the membrane through the construction of a double-layered hollow structure using a mixed material of SDC and La<sub>2</sub>NiO<sub>4</sub>. This membrane consists of a porous SDC/La<sub>2</sub>NiO<sub>4</sub> layer and a dense SDC/carbonate layer, showing a double-ring structure to enhance the bending strength of the membrane, as shown in Figure 5. The bending strength of the double-layer membrane is 84.7 MPa, which is nearly twice that of the single-layer-SDC–carbonate membrane (43.9 Mpa) [22]. Moreover, this work provides a novel approach for the fabrication of the double-layer-ceramic–carbonate hollow-fiber membrane. Even more to the point, the infiltration method of molten carbonate for the double-layer-ceramic–carbonate hollow-fiber membrane is a dip-coating technique. The infiltration method employed here bears resemblance to the vacuum-assisted technique [54] (a more accurate method for controlling the degree of the carbonate infiltration as reported by Metcalfé’s group) utilized for carbonate coating infiltration. This kind of method applied a novel way for infiltrating the carbonate into tubular or hollow-fiber membranes.



**Figure 5.** Schematic illustration of double-layer-ceramic–carbonate hollow-fiber membrane: (a) cross-section; (b) magnification of (a); (reprinted from [22] with permission of Elsevier).

## 4. External Factors and Membrane Stability

### 4.1. CO<sub>2</sub> and O<sub>2</sub> Effect

The intrinsic properties of the dual-phase membrane are fixed upon consummate preparation, serving as internal factors that remain constant. However, such external factors can be modulated according to the specific test or application requirements. The primary external factors, as illustrated by the permeation model presented in Section 2, encompass temperature and partial pressure of CO<sub>2</sub>, which directly impact the CO<sub>2</sub> permeability of the carbonate dual-phase membrane. The escalating temperature is likely to enhance CO<sub>2</sub> permeation, as the transport of carbonate and oxygen ions is a thermally activated process. Regarding the CO<sub>2</sub> partial pressure, an increase in pressure on the feed side or a decrease in pressure on the permeation side will augment the driving force of the permeation process, thereby elevating the CO<sub>2</sub> permeation flux. The impact of these two factors is regarded as a conventional understanding within the field of ceramic membranes, such as those used for oxygen transport membranes. Therefore, in this section, our primary focus will be on investigating the influence of the feed gas composition itself on both the permeation and stability aspects of the carbonate dual-phase membrane.

Since alkaline earth metals are prone to react with CO<sub>2</sub>, the performance of some carbonate dual-phase membranes based on perovskite materials may be influenced by the CO<sub>2</sub> present in the feed stream. For example, Norton et al. [55] observed that the performance of the LSCF-carbonate membrane with a thickness of 1 mm demonstrated a degradation during the CO<sub>2</sub> separation process. The CO<sub>2</sub> flux experienced a significant decrease within the temperature range of 800–900 °C subsequent to exposure to CO<sub>2</sub>/N<sub>2</sub> feed gas. The significant decline in CO<sub>2</sub> flux could be directly attributed to the formation of SrCO<sub>3</sub> resulting from the reaction between Sr in the LSCF support and CO<sub>2</sub> in the feed stream. The presence of SrCO<sub>3</sub> on the membrane surface hinders the surface reaction between CO<sub>2</sub> and O<sup>2-</sup> in the LSCF phase [56]. However, in post-combustion power plants, the presence of O<sub>2</sub> in the flue gas is generally advantageous for the CO<sub>2</sub> separation performance of the carbonate dual-phase membrane. The introduction of O<sub>2</sub> into the feed gas during the CO<sub>2</sub> separation process eliminates the formation of SrCO<sub>3</sub> in the LSCF-carbonate membrane, thereby ensuring a stable perovskite structure of LSCF [57]. Norton et al. [55] demonstrated that the LSCF-carbonate can remain stable for up to 600 h within a temperature range of 850–950 °C. Moreover, the CO<sub>2</sub> flux of approximately 3.0 mL·cm<sup>-2</sup>·min<sup>-1</sup> was 10-fold greater than that of the LSCF-carbonate membrane in the O<sub>2</sub>-free feed gas (CO<sub>2</sub>/N<sub>2</sub> feed) at 900 °C, indicating that O<sub>2</sub> can enhance the CO<sub>2</sub> permeation of the LSCF-carbonate membrane. In this instance, O<sub>2</sub> can also permeate the membrane, and in a permeation ratio of 2:1 for CO<sub>2</sub> and O<sub>2</sub>. The observed phenomenon can be attributed to the emergence of a resemblance in permeation mechanisms between the metal-carbonate and LSCF-carbonate membranes following the introduction of O<sub>2</sub> into the feed gas. The electron conductivity of LSCF (~1000 S·cm<sup>-1</sup>) significantly surpasses the CO<sub>3</sub><sup>2-</sup> conductivity (~3.5 S·cm<sup>-1</sup>) exhibited by the carbonate phase at 900 °C. Thus, the rate-limiting step of CO<sub>2</sub> transport in LSCF changed from O<sub>2</sub> conduction (~0.1 S·cm<sup>-1</sup>) to CO<sub>3</sub><sup>2-</sup> conduction after the involvement of electrons in CO<sub>2</sub> permeation [55]. The occurrence of this phenomenon is frequently observed in ceramic-carbonate membranes exhibiting a combination of mixed ion conductivity and electron conductivity.

The O<sub>2</sub>, as illustrated in the aforementioned example, not only shields certain ceramic supports from CO<sub>2</sub> assault but also actively participates in and facilitates CO<sub>2</sub> permeation throughout the process. The permeation behavior of SDC-carbonate dual-phase membranes in a feed stream containing 15% CO<sub>2</sub>-10% O<sub>2</sub>-75% N<sub>2</sub> has also been demonstrated in the study conducted by Tong et al. [17]. The SDC exhibits a markedly high O<sup>2-</sup> conductivity and an appreciably low e-conductivity under O<sup>2-</sup>-containing gas atmospheres. The study conducted by Tong et al. [17] demonstrated that a minor proportion of O<sub>2</sub> could permeate through the SDC-carbonate membrane, exhibiting a CO<sub>2</sub>:O<sub>2</sub> flux ratio of approximately 7.5:1 (not 2:1 as observed in the LSCF-carbonate membrane, CO<sub>2</sub> + 1/2O<sub>2</sub> + 2e<sup>-</sup> → CO<sub>3</sub><sup>2-</sup>). Overall, the activation of two separation mechanisms in

the ceramic–carbonate membrane can be attributed to two factors: (1) the presence of a certain  $e^-$ -conduction in the ceramic phase, and (2) the inclusion of  $O_2$  in the feed stream. Recently, some studies have reported and validated the distinct  $CO_2$  permeation pathways in perovskite ( $La_{1.5}Sr_{0.5}NiO_{4\pm\delta}$  (LSN) [53], LSCF [25]) or fluorite-based (SDC [17], ScCeSZ [58]) ceramic–carbonate dual-phase membranes in the presence of  $O_2$ .

#### 4.2. Sulfur Effect

The majority of ceramic membranes, such as perovskite membrane for  $O_2$  separation and palladium membrane for  $H_2$  separation, applied in the post- or pre-combustion process, inevitably encounter the challenges posed by sulfur. The formation of sulfur-containing gases varies across various combustion processes. The sulfur is ultimately converted to  $SO_2$  in post-combustion power plants following the combustion process. The sulfur formation, however, occurs as  $H_2S$  in the pre-combustion IGCC system. The ceramic membrane is often significantly affected by these two sulfur products, resulting in negative consequences.

For ceramic–carbonate dual-phase membranes, the impact of sulfur products may vary due to the presence of two distinct phases (i.e., ceramic and carbonate phases) within the membrane. Chen et al. [59,60] conducted an in-depth examination of the influence of sulfide gases ( $SO_2$  and  $H_2S$ ) on the SDC–carbonate membrane. The findings demonstrate a profound disparity in the impact of  $SO_2$  and  $H_2S$  on the membrane. The impact of  $SO_2$  on the SDC–carbonate membrane is primarily reflected in the degradation of the carbonate phase. The  $SO_2$  in the feed stream has the potential to undergo a reaction with the molten carbonate present in the membrane, resulting in sulfate formation. The presence of sulfate within the carbonate phase can lead to a reduction in the conductivity of carbonate ions ( $\sigma_c$ ). The effective conductivity of  $(\epsilon/\tau)_p\sigma_c$ , as discussed in Section 2.2, will exhibit a smaller value than that of  $(\epsilon/\tau)_s\sigma_i$  as the content of sulfate in the carbonate phase increases. As a result, the rate-limiting transport shifts from  $O^{2-}$ -conduction in SDC to  $CO_3^{2-}$ -conduction in the sulfated carbonate phase, which exhibits higher activation energy for electrical transport and consequently leads to a decrease in  $CO_2$  permeance. The  $SO_2$  demonstrates a negligible impact on the SDC phase, as reported by Chen et al. [59]. However, certain perovskite materials have been found to be susceptible to  $SO_2$  poisoning [61,62]. Therefore, it is imperative to consider and investigate the impact of  $SO_2$  on the perovskite-based dual-phase membrane. Among the differences from the  $SO_2$  effect, Chen et al. [60] observed that  $H_2S$  primarily exerts a detrimental influence on the ceramic phase of the SDC–carbonate membrane. The  $CO_2$  permeation flux exhibits a decline in the feed stream containing a trace amount of  $H_2S$ , attributed to the formation of Ce–O–S compounds ( $Ce_2O_2S$  and  $Ce(SO_4)_2$ ) resulting from the reaction between the SDC phase and  $H_2S$ . The presence of the Ce–O–S phase leads to a reduction in both the quantity and mobility of the lattice oxygen within the SDC phase, thereby resulting in a decrement of the  $O^{2-}$  conductivity of the SDC phase. Overall, the presence of sulfur-containing gas significantly degrades the performance and stability of the ceramic–carbonate membrane. The addition of a sulfur removal unit during the application process will adversely impact the efficiency of the dual-phase membrane.

#### 4.3. Other Impurities

The presence of sulfur-containing gas consistently exerts a detrimental impact on the performance of the dual-phase membrane. However, certain impurities may facilitate the  $CO_2$  permeation process in the carbonate dual-phase membrane. For instance,  $H_2O$  is a prevalent component in the product stream throughout the post- and pre-combustion processes. The process of steam dissolution in molten carbonates has long been acknowledged [63]. Xing et al. [64] synthesized  $CeO_2$ –carbonate dual-phase membranes, employing a series of theoretical treatments to examine the influence of steam on  $CO_2$  transport. The findings demonstrated that the dissolution of steam in the form of hydroxide ions into molten carbonates could facilitate the diffusion of  $CO_2$ . The  $CO_2$  flux of the  $CeO_2$ –carbonate membrane demonstrates an approximate 30% increment when 2.5%  $H_2O$  is introduced to the feed side, whereas a remarkable 250–300% increase in the  $CO_2$  flux is observed when

the same amount of H<sub>2</sub>O is added to the permeation side [64]. The significant escalation in CO<sub>2</sub> flux observed upon the introduction of steam can be attributed to the emergence of an additional pathway facilitating CO<sub>2</sub> transport, as illustrated in Figure 6. The transport of OH<sup>-</sup> and CO<sub>3</sub><sup>2-</sup> ions in the molten carbonate phase occurs in opposite directions, whereas the direction of the OH<sup>-</sup> ions is consistent with that of the O<sup>2-</sup> ions from the ceramic phase. In the event that the OH<sup>-</sup> transport is integrated with O<sup>2-</sup> within the solid matrix, it would lead to an enhanced electrochemical gradient of the rate-limiting step, thereby facilitating the CO<sub>2</sub> flux. The aforementioned research serves as a compelling illustration of enhancing the carbonate phase to facilitate CO<sub>2</sub> permeation.

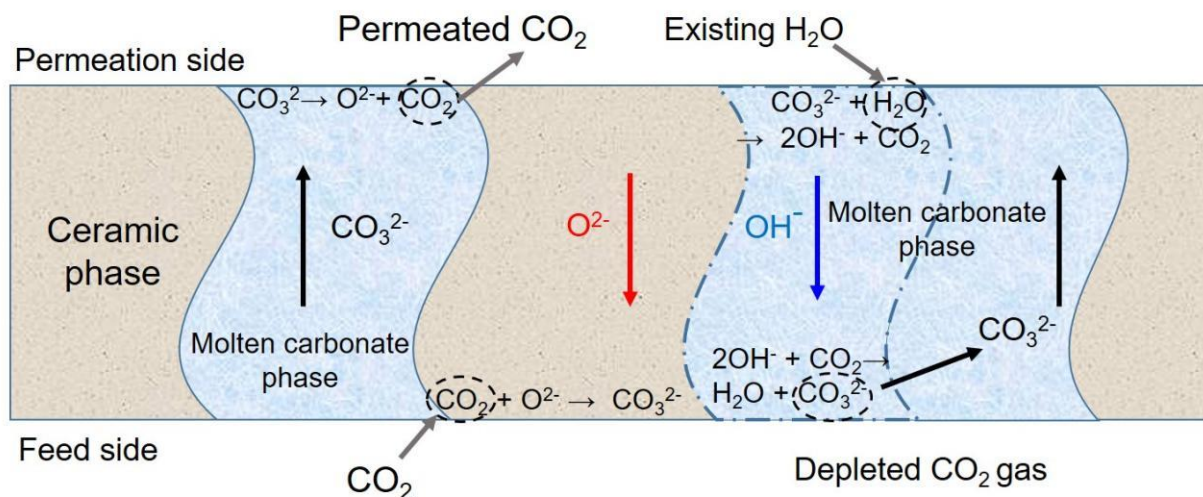


**Figure 6.** Transport model for the molten carbonate under wet conditions.

Compared to the aforementioned “passive improvement”, directly incorporating certain impurities into the carbonate phase could be termed as “active improvement”. Xing et al. [65] enhanced the CO<sub>2</sub> permeation flux by promoting the dissolution of oxide ions into the molten carbonate phase. The dissolution of CsVO<sub>3</sub> and MoO<sub>3</sub> into the molten carbonate phase resulted in an almost doubled CO<sub>2</sub> flux increase under dry operating conditions. The enhancement of oxide ion concentration and conductivity within the molten carbonate is responsible for this phenomenon. Furthermore, incorporating certain positive elements into the ceramic phase may enhance the membrane performance. For instance, Albert Gili et al. [66] examined the comparison between SDC and FSDC (Ce<sub>0.8</sub>Sm<sub>0.19</sub>Fe<sub>0.01</sub>O<sub>2-δ</sub>) containing 1.1 at% Fe, and discovered that introducing iron into SDC enhances the CO<sub>2</sub> permeability, attributed to the scavenging effect of iron on silicon-containing impurities. The molten salt was enhanced by the addition of CaCO<sub>3</sub> and BaCO<sub>3</sub>, as demonstrated by Zhang et al. [67], resulting in improved dissolved oxygen performance and enhanced permeability of the dual-phase membrane.

#### 4.4. Membrane Stability

As is the case with the majority of ceramic membranes, carbonate dual-phase membranes are typically subjected to high-temperature operations (>550 °C). The chemical stability of these membranes is compromised by the reaction between the ceramic phase and gas species such as CO<sub>2</sub> and H<sub>2</sub>S, or loss of carbonates from the support pores (e.g., metal–carbonate membranes). However, in recent years, selective and technical methods for enhancing the stability of carbonate dual-phase membranes used in CO<sub>2</sub> separation primarily include (1) application of a membrane in a suitable case, (2) support modification, (3) proper ceramic materials selection, and (4) optimal utilization of membranes. The investigations by Norton et al. [55] on LSCF–carbonate membranes (Section 4.1) and a comprehensive study of Ag–carbonate membranes (Section 3.1) serve as exemplary illustrations for enhancing membrane stability through patterns (1) and (2), respectively, as previously

mentioned. Next, we will primarily focus on presenting additional cases for investigating and enhancing the stability of the membrane.

Compared to perovskite-structured ceramics such as LSCF, fluorite-structured ceramic materials, including BYS, YSZ, and SDC, demonstrate superior stability in CO<sub>2</sub>-rich atmospheres. The BYS-carbonate membrane exhibits a “stepped” stabilization process, as illustrated in Figure 7, according to the findings of Rui et al. [44]. The CO<sub>2</sub> permeation flux demonstrates a significant increase over time, stabilizing at a constant value of 0.066 mL·cm<sup>-2</sup>·min<sup>-1</sup> after approximately 50 h. The observed phenomenon can be attributed to the gradual transformation of all rhombohedral structures in BYS into fluorite structures over time. The ionic conductivity of BYS in the fluorite structure exhibits a higher oxygen ionic conductivity than that in the rhombohedral structure, leading to an increment in the CO<sub>2</sub> flux during the long-term stability test [44]. The transient transformation process of the BYS support is more conducive to CO<sub>2</sub> transportation and membrane stabilization. Lu and Lin conducted an investigation on the stability of the asymmetric YSZ-carbonate membrane [46]. The CO<sub>2</sub> flux through the membrane remains constant at 650 °C throughout the approximately 20 h operation period. The morphological integrity of the YSZ-carbonate membrane following the high-temperature CO<sub>2</sub> permeation test remains consistent with that prior to the test, suggesting excellent chemical compatibility and stability between YSZ and carbonate at elevated temperatures. Norton et al. [24] investigated the CO<sub>2</sub> permeation characteristics and long-term stability of the disk SDC-carbonate dual-phase membrane under high-temperature CO<sub>2</sub>/N<sub>2</sub> and simulated syngas feed conditions. The results presented in Figure 8a demonstrate that the SDC-carbonate membrane exhibits a consistent CO<sub>2</sub> permeation flux of approximately 0.42 mL·cm<sup>-2</sup>·min<sup>-1</sup> over an extended period of 80 h at 700 °C, under a CO<sub>2</sub> partial pressure of 2.5 atm in a 50% CO<sub>2</sub>/50% N<sub>2</sub> feed gas mixture. Atmospheric pressure conditions prevail, resulting in a CO<sub>2</sub> flux of approximately 0.7 mL·cm<sup>-2</sup>·min<sup>-1</sup> for over 330 h at 900 °C, with a CO<sub>2</sub> partial pressure of 0.5 atm in the CO<sub>2</sub>/N<sub>2</sub> feed gas [24]. Moreover, regarding the simulated fuel gas composition, consisting of 50% CO, 35% CO<sub>2</sub>, 10% H<sub>2</sub>, and 5% N<sub>2</sub>, the CO<sub>2</sub> permeation flux was maintained at 0.4 mL·cm<sup>-2</sup>·min<sup>-1</sup> at 700 °C for a duration of 5 days, while being exposed to a total feed pressure of 3 atm with a CO<sub>2</sub> partial pressure of 1.8 atm, and the CO<sub>2</sub> flux was approximately 0.31 mL·cm<sup>-2</sup>·min<sup>-1</sup> at a temperature of 700 °C under atmospheric pressure, with a CO<sub>2</sub> partial pressure of 0.35 atm, as depicted in Figure 8b. Importantly, the XRD patterns of the SDC-carbonate membrane surface after long-term testing revealed that the sweep side of the membranes maintained a pristine fluorite structure, whereas only minor peaks corresponding to Sm<sub>2</sub>O<sub>3</sub> were observed on the feed side. The findings imply that the SDC-carbonate membrane demonstrates exceptional permeation stability when exposed to H<sub>2</sub> or CO<sub>2</sub>/N<sub>2</sub> feeds. Indeed, several other studies pertaining to the SDC-carbonate membrane have also corroborated the exceptional stability of the SDC phase within this domain.

The selection of appropriate ceramic materials can enhance the stability of the carbonate dual-phase membrane; however, nearly all ceramic membranes are susceptible to varying degrees of sulfur-containing gas-induced degradation. In particular, the presence of H<sub>2</sub>S significantly impacts the ceramic material during the pre-combustion process in the presence of H<sub>2</sub>. Recently, Chen et al. [68] developed an asymmetric membrane, primarily composed of an adsorbed layer (SDC/BYS or SDC porous layer) for H<sub>2</sub>S removal and a dense ceramic-carbonate layer (SDC-carbonate dense layer) for CO<sub>2</sub> separation, as illustrated in Figure 9. The function of BYS is to prevent the infiltration of molten carbonate into the pores of the adsorbed layer, owing to its non-wettability toward carbonates. The findings revealed that the utilization of asymmetric membranes significantly enhances the stabilization period of membrane separation (ranging from 10 to 12 times the stability duration of a single SDC-carbonate membrane). As illustrated in Figure 10a, the asymmetric membranes exhibit stable performance within a H<sub>2</sub>S-containing atmosphere, contrasting the instability of single-layer membranes. The development of a “saturation adsorption point” for H<sub>2</sub>S removal was observed in the asymmetric membrane during the CO<sub>2</sub> sep-

aration process, leading to a decline in the performance of CO<sub>2</sub> separation beyond this point. However, the adsorbed layer can be efficiently regenerated within a short duration at 850 °C in an oxygen-enriched gas stream [68] (refer to Figure 10b). The stripped sulfur from the adsorbed layer during the regeneration process can be collected as an elemental sulfur product, enhancing the efficiency and value of this membrane for CO<sub>2</sub> capture in the pre-combustion IGCC application.

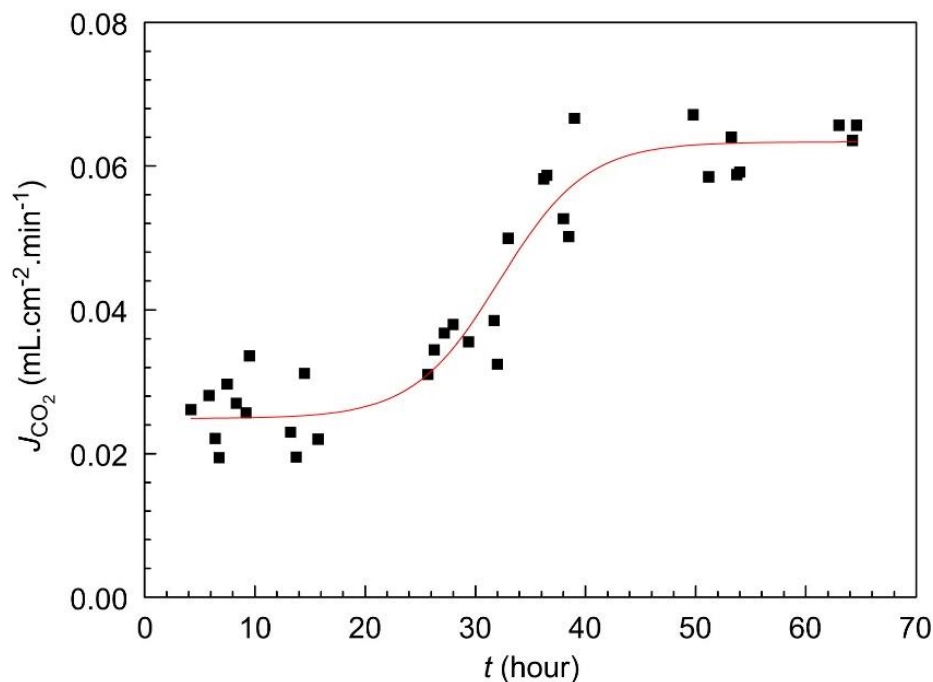


**Figure 7.** Time dependence of CO<sub>2</sub> flux through the BYS-carbonate dual-phase membrane at 650 °C (reprinted from [44] with permission of Elsevier).

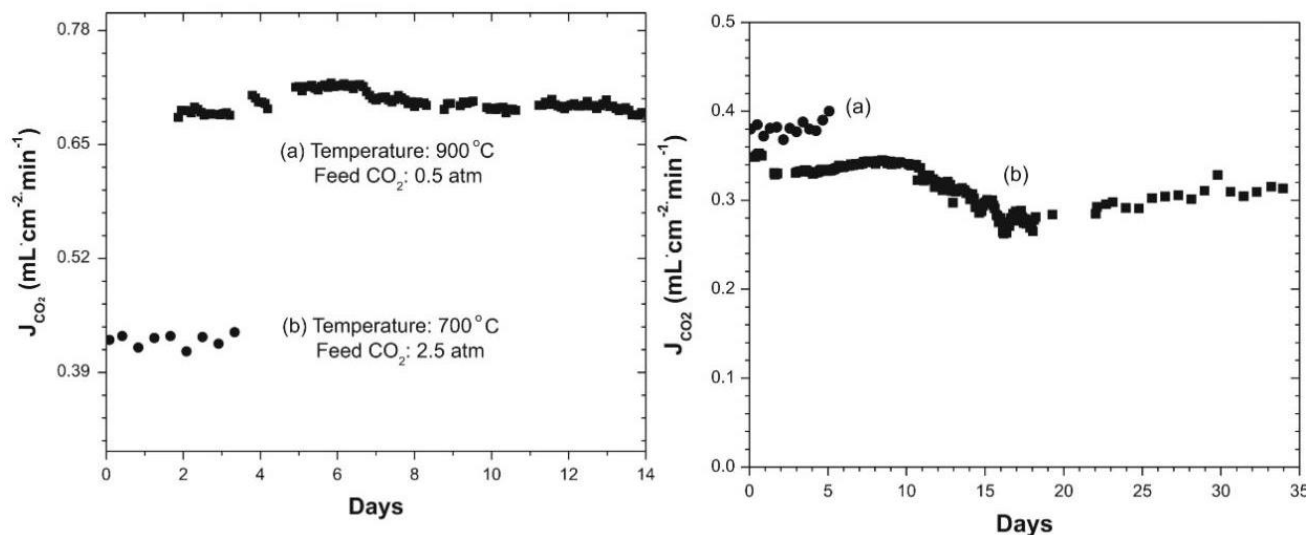


**Figure 8.** Time dependence of CO<sub>2</sub> permeation flux of SDC-carbonate membrane: (a) 50% CO<sub>2</sub>/50% N<sub>2</sub>; (b) simulated syngas feed (50% CO, 35% CO<sub>2</sub>, 10% H<sub>2</sub>, and 5% N<sub>2</sub>) at 700 °C (curve-a is high-pressure feed at total feed pressure of 3 atm with 0.18 atm CO<sub>2</sub> partial pressure; curve-b is atmospheric pressure feed with 0.35 atm CO<sub>2</sub> partial pressure) (reprinted from [24] with permission of Elsevier).

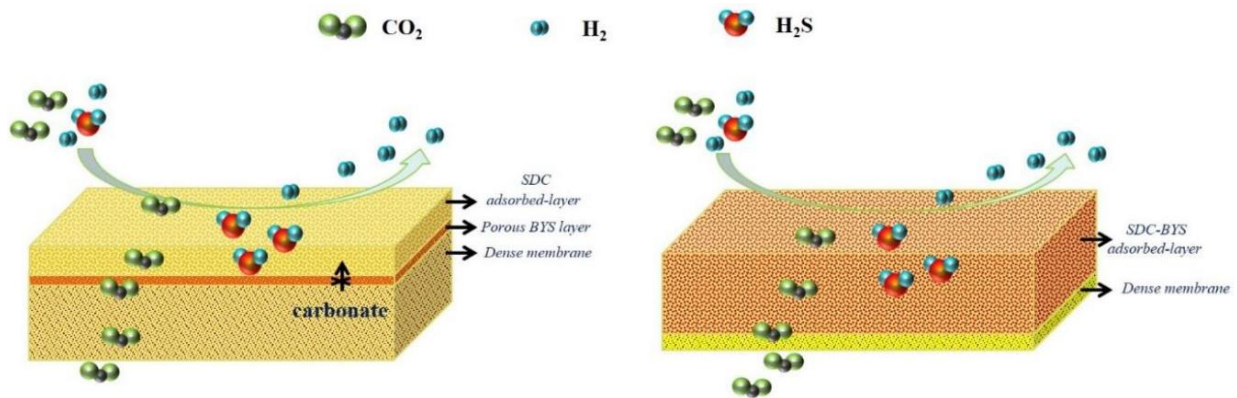


**Figure 9.** Schematic of asymmetric membranes for CO<sub>2</sub> separation from a H<sub>2</sub>S-containing gas mixture (reprinted from [68] with permission of Elsevier).

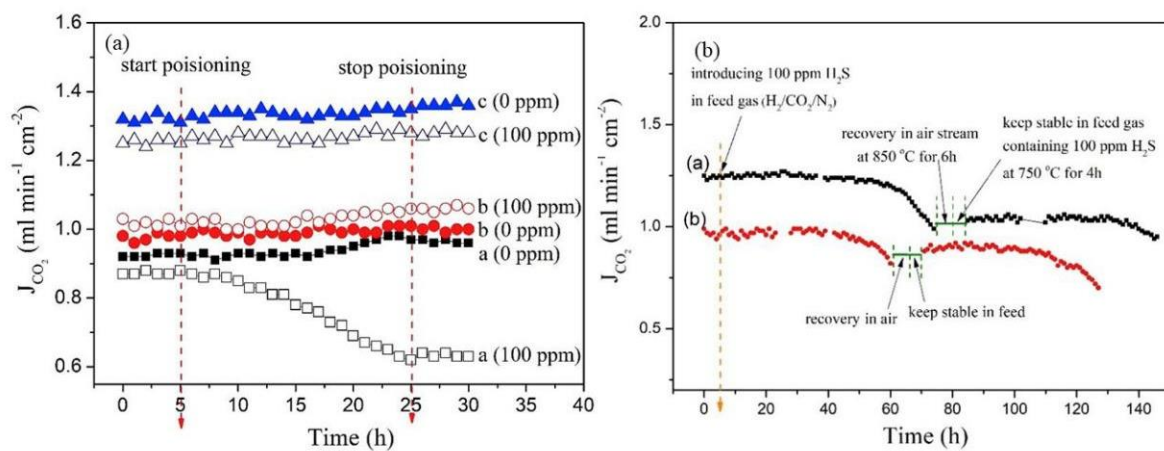


**Figure 10.** CO<sub>2</sub> permeation stability of membranes with H<sub>2</sub>/CO<sub>2</sub>/N<sub>2</sub> mixture feed containing 0 or 100 ppm H<sub>2</sub>S at 750 °C: (a) comparison of three different membranes (curve-a is single SDC-carbonate membrane; curve-b is SDC(porous)-BYS-SDC/carbonate membrane; curve-c is SDC/BYS(porous)-SDC/carbonate membrane), (b) Sulfur-resistant stability and regeneration capacity of the asymmetric membranes (curve-a is SDC(porous)-BYS-SDC/carbonate membrane; curve-b is SDC/BYS(porous)-SDC/carbonate membrane) (reprinted from [68] with permission of Elsevier).

## 5. Applications of Membrane

### 5.1. Basic Assessment in Post- and Pre-Combustion Processes

The approaches for CO<sub>2</sub> capture from power plants can be fundamentally categorized into three processes: post-combustion, which involves capturing CO<sub>2</sub> from flue gases; pre-combustion, which entails capturing CO<sub>2</sub> from high-pressure syngas (H<sub>2</sub> + CO); and oxy-fuel, which involves combusting with pure O<sub>2</sub>. Due to its high operating temperature (>500 °C), the metal- or ceramic-carbonate dual-phase membrane exhibits competitiveness compared to certain conventional processes, such as the MEA process and Selexol process are employed for CO<sub>2</sub> capture in combustion processes, including Oxy-fuel, and pre- and post-combustion. The dual-phase membranes have the potential to be employed in the purification of oxy-fuel combustion flue gas containing a concentrated CO<sub>2</sub> stream. However, dense inorganic oxygen transport membranes (OTMs), being a well-established membrane for O<sub>2</sub> separation, could also serve as a viable option in the oxy-combustion process [68–71]. Owing to this end, the carbonate dual-phase membranes are primarily contemplated in the post- and pre-combustion processes at present.

The driving force for the dual-phase membranes lies in the gradient of CO<sub>2</sub> electrochemical potential that exists across their opposing surfaces. The CO<sub>2</sub> separation process does not require electricity, rendering it a promising, low-cost, and energy-efficient option

for carbon capture. The CO<sub>2</sub> concentration and partial pressure should be primarily considered to assess the suitability of the membranes in different scenarios. Table 8 enumerates the typical gas compositions in various combustion scenarios. As shown, the CO<sub>2</sub> concentration of the natural-gas-combusted flue gas is relatively low during the post-combustion process, leading to an inadequate chemical potential gradient of CO<sub>2</sub> between the feed side and the permeation side. Furthermore, although the flue gas resulting from natural gas combustion possesses an optimal operational temperature for CO<sub>2</sub> separation using the carbonate dual-phase membrane, it is characterized by a low-pressure level equivalent to atmospheric pressure. The gas stream must be compressed before separation. Therefore, prior to separation, it is imperative to compress the flue gas. Typically, the flue gas should be cooled to room temperature and subsequently compressed to increase pressure in order to minimize compression workload. The carbonate dual-phase membrane technology for CO<sub>2</sub> separation in this case incurs a higher energy penalty (2.5–3.5% points) compared to MEA-based post-combustion capture [72]. The potential application of dual-phase membranes in the separation of coal-fired flue gas, characterized by its relatively high CO<sub>2</sub> concentration (above 10%), could offer an innovative solution for CO<sub>2</sub> capture. The impact of SO<sub>2</sub> from coal combustion on membrane performance must be taken into account, as previously mentioned in Section 4.1, due to its adverse effects. The additional energy penalty from heat exchange will be further increased, as the removal of SO<sub>2</sub> typically occurs at a lower temperature compared to the high operating temperature of the dual-phase membrane.

**Table 8.** The typical gas compositions of different combustion cases.

Gas Type	Combustion Process	Composition/Vol	Ref.
Natural-Gas-fired flue gas	Post-combustion	~4 to 8% CO <sub>2</sub> ; ~14% H <sub>2</sub> O; ~4% O <sub>2</sub> ; 73–74% N <sub>2</sub> ; trace CO and NO <sub>x</sub>	[73,74]
Coal-fired flue gas	Post-combustion	~13% CO <sub>2</sub> ; ~6% H <sub>2</sub> O; ~4% O <sub>2</sub> ; 76–77% N <sub>2</sub> ; trace CO, NO <sub>x</sub> and SO <sub>2</sub>	[73,74]
Syngas from gasifier outlet	Pre-combustion (IGCC)	~18% CO <sub>2</sub> ; 9.0% H <sub>2</sub> O; ~28% H <sub>2</sub> ; ~41% CO; trace CH <sub>4</sub> , H <sub>2</sub> S, N <sub>2</sub> , Ar, As and Hg	[75,76]
Shifted gas from Water—Gas Shift process (WGS)	Pre-combustion (IGCC)	~28 to 38% CO <sub>2</sub> ; ~12 to 26% H <sub>2</sub> O; ~43 to 56% H <sub>2</sub> ; ~1 to 5% CO; trace H <sub>2</sub> S and N <sub>2</sub>	[76,77]

The implementation of a carbonate dual-phase membrane in the pre-combustion process confers a competitive edge. As shown in Table 8, higher CO<sub>2</sub> concentrations, a positive condition for the dual-phase membrane, can be applied in the pre-combustion IGCC case, not only for the syngas, but also for the shifted gas. The CO<sub>2</sub> capture in this process is generally operated at a high-pressure (35–40 bar) gas stream, which is also suitable for the carbonate dual-phase membrane. Currently, the Selexol or Rectisol absorption approach is the preferred CO<sub>2</sub> capture process. However, it is expected to result in an approximate 30% increase in the levelized cost of electricity with a 90% CO<sub>2</sub> capture rate [78]. Table 9 presents a comparative analysis of the net efficiency of CO<sub>2</sub> capture from IGCC plants, employing both Selexol and ceramic CO<sub>2</sub>-selective membranes. The ceramic (porous or dual-phase) membranes, as illustrated, exhibit a significantly higher net efficiency. Anantharaman et al. [72] revealed that the overall process efficiency of a two-stage process based on a dual-phase membrane outperforms the Selexol process by approximately 2.15% points. A simplified flow diagram illustrating a two-stage dual-phase membrane process is presented in Figure 11, based on the findings reported by Anantharaman's research group. The first stage membrane is positioned downstream of the high-temperature shift (HTS) water–gas shift process. The first stage dual-phase membrane is employed to capture a portion of the CO<sub>2</sub> generated from the HTS product. Due to the isolation of one of the reaction products (CO<sub>2</sub>), the equilibrium is redistributed, enabling the conventional low-temperature shift (LTS) water–gas shift process to be supplanted by an alternative high-temperature shift (HTS) procedure. The aforementioned mechanism can persistently maintain an elevated temperature, thereby facilitating the utilization of a

second-stage dual-phase membrane at an optimal operating temperature. The separation of residual CO<sub>2</sub> occurs in this stage. Potential challenges in the initial stages of deep CO<sub>2</sub> removal could significantly exacerbate the difficulty of CO<sub>2</sub> separation in subsequent stages. Therefore, the utilization of H<sub>2</sub>-selective membranes during the initial stage can enhance both CO conversion and CO<sub>2</sub> concentration, thereby improving the overall efficiency. As mentioned above, the application of a dual-phase membrane can enhance process efficiency, attributable to the optimized heat exchange and gas compression penalties within the process, thereby eliminating the need for cooling and heating cycles.

**Table 9.** Comparison of Selexol and ceramic CO<sub>2</sub>-selective membrane in IGCC plant.

Ref.	Capture Technology	Net Efficiency/%-LHV	Energy Penalty/%-Point
[79]	Selexol	36.79	6.7
	porous ceramic membrane	38.38	5.0
[72]	Selexol	36.66	6.8
	Carbonate dual-phase membrane	38.82	4.6

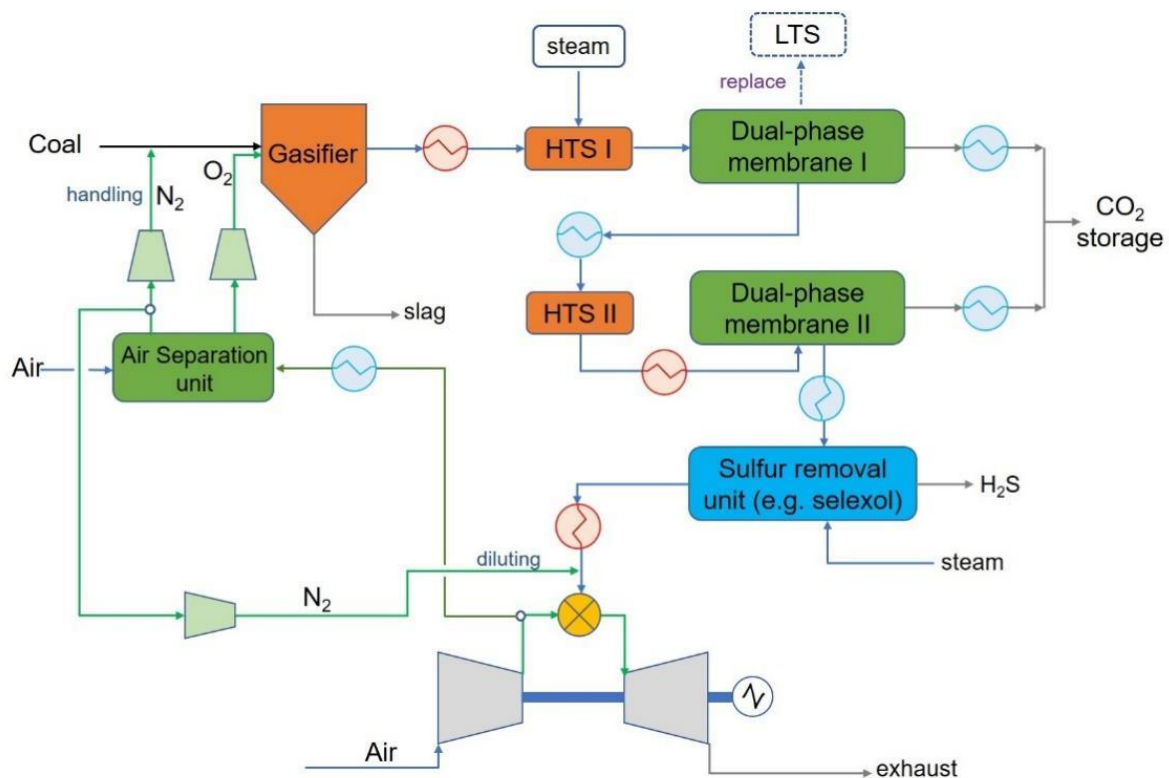


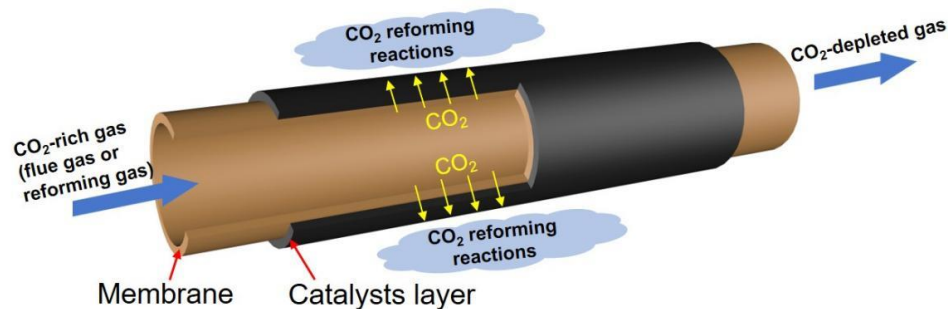
**Figure 11.** Process flow diagram of IGCC process with CO<sub>2</sub> capture using dual-phase membrane.

The carbonate dual-phase membrane demonstrates superior performance to the Selexol membrane reported by Anantharaman et al. [72]. This evaluation is based on the assumption that H<sub>2</sub>S will not have any adverse effects on the separation process. However, the presence of H<sub>2</sub>S in the pre-combustion IGCC case poses an inevitable challenge that hampers the efficient separation of the aforementioned dual-phase membrane. If this were the scenario, the application of H<sub>2</sub>S removal technology, such as the Selexol process, should be implemented upstream of the carbonate dual-phase membrane. This will result in process inefficiencies. Fortunately, Chen et al. [68] recently proposed a novel approach to address the H<sub>2</sub>S issue, as mentioned previously. The optimized asymmetric membrane has the potential to achieve simultaneous H<sub>2</sub>S removal and CO<sub>2</sub> separation functionality following the enhancement of its material and structure. The H<sub>2</sub>S problem can thus be disregarded during the application of the dual-phase membrane.

### 5.2. Membrane Reactor Concept

The operating temperature range (500–900 °C) of the dual-phase membrane for CO<sub>2</sub> separation is also well suited for certain high-temperature catalytic reactions. Thus, with the integration of dual-phase membranes with catalysts to the fabrication of membrane reactors, facilitating simultaneous separation and reaction processes, the application of dual-phase membranes appears to be a favorable choice. The dual-phase membrane reactors are currently employed in two operational modes, as follows: The reactor wall is fabricated from a carbonate dual-phase membrane, with a suitable catalyst being either packed or sintered within the membrane reactor. In the first mode, the most extensively studied configuration of a dual-phase membrane reactor involves coupling a CO<sub>2</sub> reforming reaction at the permeation side to convert the permeated CO<sub>2</sub> (refer to Figure 12a). In this manner, the catalytic reaction rapidly consumes the separated CO<sub>2</sub> as a reactant, thereby providing an additional “sweeping power” to elevate the partial pressure of CO<sub>2</sub> (i.e., the driving force for permeation). The coupling mode under examination exhibits a significant propensity to facilitate the separation process.

(a)



(b)

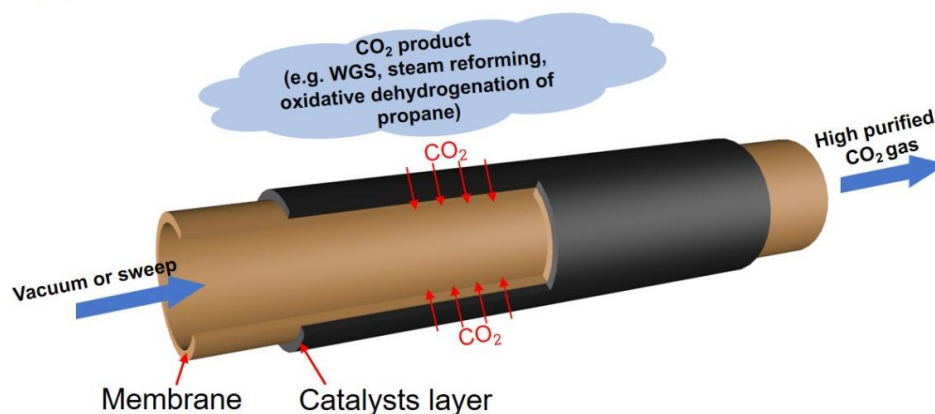


**Figure 12.** Two modes of the dual-phase membrane reactors at present: (a) The permeation side couple a CO<sub>2</sub> reforming reaction, (b) Reaction to produce CO<sub>2</sub>.

Anderson and Lin pioneered the proposal of a ceramic (using LSCF)–carbonate dual-phase membrane reactor for CH<sub>4</sub> dry reforming, enabling in situ separation to capture CO<sub>2</sub> as a reactant [77], as shown in Figure 13. Under the reaction conditions of 850 °C, a feed gas consisting of 25% CO<sub>2</sub> and 75% N<sub>2</sub> at a flow rate of 10 mL min<sup>−1</sup>, and a sweep gas composed of 50% CH<sub>4</sub> using a traditional Ni/λ-alumina catalyst, demonstrated a CO<sub>2</sub> flux of 0.17 mL·cm<sup>−2</sup>·min<sup>−1</sup>, a H<sub>2</sub> production rate of 0.3 mL·cm<sup>−2</sup>·min<sup>−1</sup>, and a conversion

of CO<sub>2</sub> and CH<sub>4</sub>, respectively, of 88.5 and 8.1%. Zhang et al. [80] employed CeO<sub>2</sub>-based ceramic materials (GDC, SDC) to fabricate a ceramic-carbonate membrane reactor for the dry reforming of CH<sub>4</sub>. The Ni-MgO-1wt% Pt catalyst-based GDC-carbonate membrane reactor achieved a CO<sub>2</sub> flux of 2.25 mL·cm<sup>-2</sup>·min<sup>-1</sup>, a H<sub>2</sub> and CO production rate of 3.75 and 3.24 mL·cm<sup>-2</sup>·min<sup>-1</sup>, respectively, and a CH<sub>4</sub> conversion of 93.9% at 850 °C. Compared to the LSCF-carbonate membrane reactor, the GDC-carbonate membrane reactor exhibits significantly improved performance attributed to three key factors as follows: (1) ceramic materials with enhanced stability and superior oxygen conduction (such as SDC, GDC compared to LSCF); (2) the integration of a superior catalyst; and (3) optimal permeation conditions (balanced feed and sweep gas compositions). The interaction between LSCF and carbonate led to a suboptimal performance of the LSCF-carbonate membrane reactor. In contrast, GDC demonstrated more stability under CO<sub>2</sub>-enriched conditions. The integration of a superior catalyst will potentiate the conversion of the CO<sub>2</sub>-consuming catalytic reaction, thereby escalating the CO<sub>2</sub> permeation from the feed side. The increase in permeable CO<sub>2</sub> can further enhance the conversion of CH<sub>4</sub>. This phenomenon of a “virtuous circle” in the membrane reactor has been substantiated by the aforementioned two studies. For the CH<sub>4</sub> reforming membrane reactor, Zhang et al. [81,82] concurrently fabricated SDC-NiO-carbonate and Ag-carbonate membrane reactors for simultaneous CO<sub>2</sub>-O<sub>2</sub> capture and in situ dry-Oxy CH<sub>4</sub> reforming. The two membrane reactors under investigation exhibit high CO<sub>2</sub> permeation flux (1.17–2.4 mL·cm<sup>-2</sup>·min<sup>-1</sup>), production rate (with a maximum H<sub>2</sub> and CO production rate of approximately ~4 mL·cm<sup>-2</sup>·min<sup>-1</sup>), and CH<sub>4</sub> conversion rate (80–85%) under optimal experimental conditions. Fabián-Anguiano et al. [27] have employed the CO<sub>2</sub>/O<sub>2</sub> co-permeation property to develop a membrane reactor for dry methane reforming and methane partial oxidation in a single-stage process, demonstrating excellent performance under high-temperature conditions. The membrane reactors, based on the CO<sub>2</sub>/O<sub>2</sub> co-permeation character revealed by Norton et al. [55], demonstrate significant potential for the separation of CO<sub>2</sub> from flue gas, providing a promising approach for the application of carbonate dual-phase membranes in the post-combustion process. In addition to the aforementioned dry reforming membrane reactors, Chen et al. [83] first proposed an SDC/LaNiO<sub>3</sub>(LNO)-carbonate dual-phase membrane reactor integrated with a La<sub>0.9</sub>Ce<sub>0.1</sub>NiO<sub>3-δ</sub> (LCNO) catalyst for simultaneous CO<sub>2</sub> separation and reverse water-gas shift (RWGS) reaction (CO<sub>2</sub> + H<sub>2</sub> ⇌ CO + H<sub>2</sub>O). The separated CO<sub>2</sub> from the feed side can be rapidly consumed by the H<sub>2</sub> of the sweep side. The results reveal that the CO<sub>2</sub> permeation flux in the membrane reactor with a 10% H<sub>2</sub>/He gas sweep is approximately four times higher (1.04 versus 4.25 mL·cm<sup>-2</sup>·min<sup>-1</sup>) than that of a single CO<sub>2</sub> separation process utilizing pure He sweeping. Zhu et al. [84] reported an SDC-carbonate dual-phase membrane reactor coupling of CO<sub>2</sub> separation with CO<sub>2</sub> methanation reaction over a Ni-based catalyst. In general, the carbonate dual-phase membrane reactors based on the first mode (refer to Figure 12a) primarily emphasize enhancing CO<sub>2</sub> capture through its coupling with the CO<sub>2</sub> reforming reaction.

The second frequently examined mode of carbonate dual-phase membrane reactors involves the integration of a catalytic reaction with CO<sub>2</sub> separation capabilities, aimed at extracting the CO<sub>2</sub> product from the reactor, as depicted in Figure 12b. The removal of generated CO<sub>2</sub> will enhance the conversion of the catalytic reaction, which is limited by thermodynamic equilibrium, leading to an augmented yield of the desired product. The prerequisites for the implementation of dual-phase membrane reactors based on the second mode necessitate the employment of active catalysts to alleviate the burden of the separation process. The dual-phase membrane separators require a high CO<sub>2</sub> permeation flux and selectivity to ensure that the reaction rate aligns with the permeation rate. Furthermore, certain membrane reactors sans catalysts rely solely on the membrane wall, which exhibits catalytic activity and participates in the reaction, to regulate the reaction mechanism. The overall performance of this membrane reactor system not only enhances the desired product yield and selectivity but also minimizes the subsequent separation process required for the recovery of reactants or the isolation of carbon dioxide from the product stream.

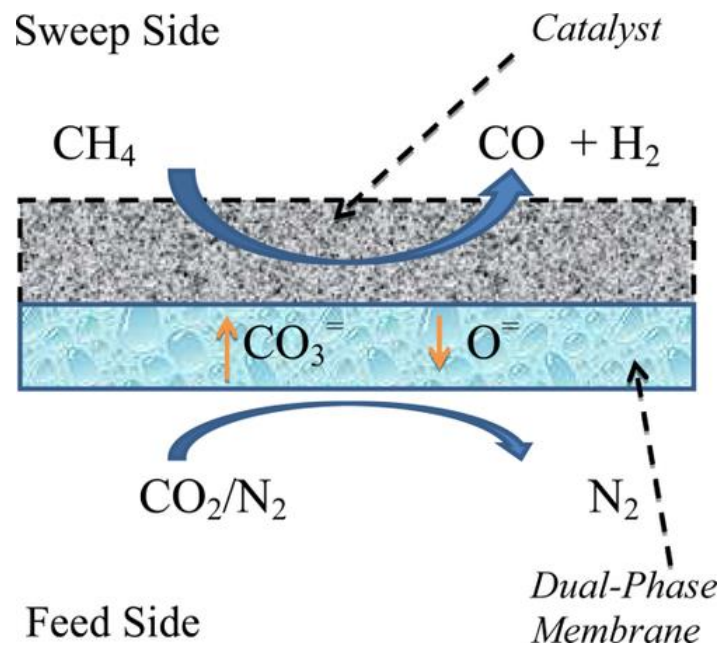


**Figure 13.** Schematic illustration of membrane reactor with ceramic-carbonate dual-phase membrane coupling CO<sub>2</sub> separation with CH<sub>4</sub> dry reforming (reprinted from [77] with permission of Wiley-Blackwell).

Based on the second reactor mode, a prime example is the dual-phase membrane reactor constructed from a tubular SDC-carbonate membrane, as reported by Dong and Lin [85], as illustrated in Figure 14. The membrane reactor is employed for the water-gas shift (WGS) reaction ( $\text{CO} + \text{H}_2\text{O} \rightleftharpoons \text{CO}_2 + \text{H}_2$ ), while enabling in situ separation of CO<sub>2</sub>. The SDC-carbonate membrane reactor, effectively eliminates CO<sub>2</sub> from the WGS product stream without the need for a catalyst, thereby promoting the conversion of CO to H<sub>2</sub> at elevated temperatures. The findings demonstrate that the catalytic-free SDC-carbonate membrane reactor achieves a CO<sub>2</sub> flux of  $2.7 \times 10^{-3} \text{ mol}\cdot\text{m}^{-2}\cdot\text{s}^{-1}$ , along with CO conversion and CO<sub>2</sub> recovery rates of 26.1% and 18.7%, respectively, at 900 °C. These outcomes notably outperform the conventional fixed-bed reactor under identical conditions. As previously discussed, the ceramic-carbonate membrane demonstrates enhanced suitability for CO<sub>2</sub> capture in the pre-combustion IGCC scenario. This membrane reactor concept gives a demonstration of the feasibility of a high-efficiency IGCC power plant with CO<sub>2</sub> capture. Another instance is the steam reforming of methane (SRM) reactor, which is based on a thin BYS/SDC-ceramic-carbonate membrane as reported by Wu et al. [86]. The production of CO<sub>2</sub> can be considered as a byproduct in the SRM reaction process, which also encompasses the WGS reactions ( $\text{CH}_4 + \text{H}_2\text{O} \leftrightarrow \text{CO} + 3\text{H}_2$ ;  $\text{CO} + \text{H}_2\text{O} \leftrightarrow \text{CO}_2 + \text{H}_2$ ;  $\text{CH}_4 + 2\text{H}_2\text{O} \leftrightarrow \text{CO}_2 + 4\text{H}_2$ ). The membrane reactor achieves a hydrogen yield of 90% with a CO<sub>2</sub> recovery rate of 84% at a temperature of 900 °C and feed pressure of 1 atm, demonstrating significant superiority over the conventional fixed-bed reactor operating under similar conditions. The performance of this reactor significantly surpasses that of the conventional fixed-bed reactor under similar conditions, demonstrating its superiority in terms of efficiency and functionality. The removal of CO<sub>2</sub> from the H<sub>2</sub>-product stream through the thin BYS/SDC-carbonate membrane reactor can enhance the H<sub>2</sub> concentration while simultaneously reducing CO and CO<sub>2</sub> in the retentate stream. Thus, the dual-phase reactor can notably alleviate the production process as no extra WGS unit is needed.

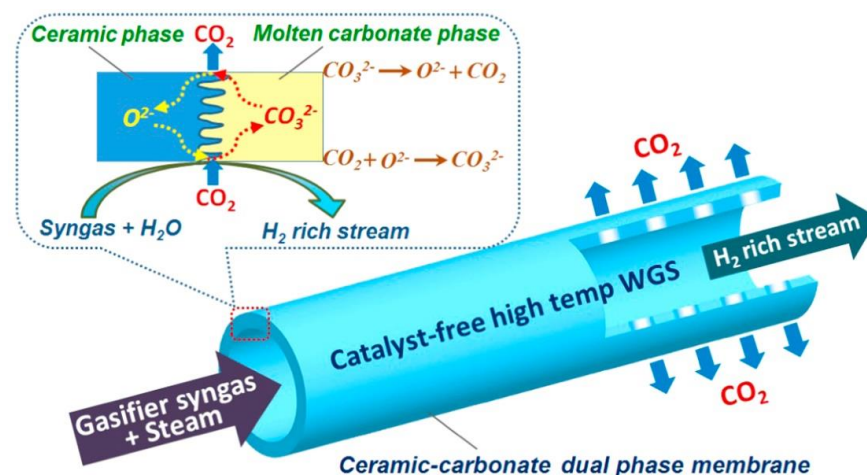


**Figure 14.** Schematic of ceramic–carbonate dual-phase membrane reactor for syngas WGS reaction (reprinted from [85] with permission of Elsevier).

## 6. Perspective

Although significant advancements have been reported in the development of carbonate dual-phase membranes, several pressing challenges must be addressed to meet the demands of future applications. At present, the development of prominent handles for CO<sub>2</sub> separation in dual-phase membranes primarily involves (1) the creation of novel materials, (2) chemical stability, (3) moderate permeability, (4) mechanical strength, and (5) configuration and high-temperature sealing. In the ensuing sections, we delve into the pivotal challenges and prospective development trajectories of carbonate dual-phase membranes.

### 6.1. Main Issues

Perovskite structure materials, representing a significant subset of ceramic materials, typically incorporate alkaline earth elements such as Ca, Sr, and Ba. However, the propensity of CO<sub>2</sub> to react with the alkaline earth elements is heightened at elevated temperatures. Perovskites containing conventional metals, such as cobalt, are also prone to instability in CO<sub>2</sub>-rich environments. The enrichment of cobalt can reduce electronegativity, thereby enhancing the basicity of perovskite materials, leading to facilitated reactions with CO<sub>2</sub>. The availability of ceramic materials suitable for the preparation of dual-phase membranes for high-temperature CO<sub>2</sub> separation is constrained. The choice of materials for the support synthesis of the dual-phase membrane should prioritize stability, ensuring retention of its phase structure in the presence of a CO<sub>2</sub>-enriched atmosphere at elevated temperatures. The primary constraint on the chemical stability of the dual-phase membrane is attributed to the interactions between its components. Presently, as previously mentioned, SDC demonstrates optimal performance in terms of permeance and stability. However, the selection of the dual-phase membrane is rather restrictive. Thus, the development of novel and more reliable membrane materials is crucial for adapting to CO<sub>2</sub>-rich atmospheres at high temperatures, thereby ensuring chemical stability during long-term operations.

The permeation flux or permeance of the carbonate dual-phase membrane remains moderate when compared to that of the O<sub>2</sub> transport membrane (OTM). The O<sub>2</sub> flux of certain oxygen-permeable membranes often achieves values of up to 10–15 mL·cm<sup>-2</sup>·min<sup>-1</sup> [87], whereas the maximum CO<sub>2</sub> flux of the SDC–carbonate dual-phase hollow-fiber membrane, as reported by Chen et al. [51], is approximately 5 mL·cm<sup>-2</sup>·min<sup>-1</sup> at present. Although this ceramic–carbonate hollow-fiber membrane offers superior CO<sub>2</sub> permeance, its mechanical strength is inadequate due to its small thickness and big porosity. Porousness and the presence of liquid carbonate within the pores of the membrane can exacerbate the vulnerability of the dual-phase membrane. The plate (or planar) and tubular membranes exhibit a relatively higher mechanical strength compared to hollow fibers. Nonetheless, the CO<sub>2</sub> flux of these two configurations remains moderate. Currently, a continuous re-

finement of the carbonate dual-phase membrane structure is required to achieve both enhanced mechanical robustness and CO<sub>2</sub> permeability. For instance, Jin and colleagues demonstrated that the mechanical strength of multi-channel (4-channel and 19-channel) O<sup>2-</sup>-transport hollow-fiber membranes was approximately 6 to 60 times stronger than that of a single hollow-fiber membrane, while the O<sub>2</sub> flux was approximately two times higher than that of single membranes under similar conditions [88,89]. The findings imply that a multi-channel structure can augment the mechanical robustness of pure ceramic hollow fibers. However, for the carbonate dual-phase membranes, the validity of this approach requires further verification due to the presence of pores and the molten carbonate phase. The implementation of a multi-channel structure will result in a compromised packing density, as observed in a comparison between a single-channel variant (~3000 m<sup>2</sup>·m<sup>-3</sup>) and a 19-channel configuration (~800 m<sup>2</sup>·m<sup>-3</sup>) [89]. Thus, the balance between configuration, packing density, and mechanical strength must be maintained in future applications to optimize the trade-off relationship.

The carbonate dual-phase membranes frequently encounter sealing issues under elevated temperatures. The dual-phase membrane, particularly the ceramic-carbonate variety, exhibits a significant expansion in response to rising temperatures. Thus, the high-temperature sealants must be compatible with the thermal expansion coefficient of the dual-phase membranes to maintain the integrity of the membrane at elevated temperatures. The sealing of carbonate dual-phase membranes involves two types of materials. The first type refers to metal pastes or rings, such as silver and gold [90–92]. This type of sealant requires high-temperature pre-treatment (~900 °C) to achieve a smooth and dense texture. Nonetheless, this method is rather costly and the membranes are prone to cracking during the cooling process due to the disparate thermal coefficients between metals and ceramics. Furthermore, the application of metal paste sealants could potentially alter the separation mechanism and its resulting consequences. A pure ionic ceramic-carbonate membrane, for instance, exhibits selectivity for CO<sub>2</sub> permeation alone. However, the O<sub>2</sub> will also permeate the membrane due to the introduction of electrons from the metal sealant. This may pose challenges during the application process.

The other type involves a ceramic paste or a blend of ceramic-glass sealant [93–96]. The composition of ceramic-glass sealant is not uniform, necessitating the adjustment of various membrane materials based on their distinct thermal expansion coefficients. This sealant requires a pre-treatment process before being applied, which is contingent on the melting and softening points of various ceramic-glasses. In the meantime, the ceramic sealants should be an inert component relative to the membrane material. In addition to the selection of high-temperature sealants, the configurations of the dual-phase membrane also contribute to the sealing process. For instance, the construction of multiple planar membrane stacks can be employed to amplify the membrane area, thereby facilitating large-scale integration. The challenges in achieving a secure seal for planar membranes arise from the placement of the membrane and sealant within the high-temperature core. In contrast, tubular and hollow-fiber membranes offer a solution to this issue, as the sealing position can be relocated beyond the high-temperature heating zone. However, the current approach leads to an incomplete utilization of the membranes, as portions of the membranes lie outside the heating zone. The consequence of this is an escalated expenditure associated with the separation process. Thus, as discussed previously, it is imperative to further advance the high-temperature sealants and sealing techniques to augment the stability of the carbonate dual-phase membranes.

## 6.2. Membrane Development

The fundamental challenge of carbonate dual-phase membranes achieves superior permeance. The majority of research efforts dedicated to the development of the dual-phase membrane are primarily focused on addressing this issue in order to achieve the threshold of industrial application. However, it is crucial to maintain a balance between CO<sub>2</sub> permeation flux and membrane structure. A decrease in membrane thickness enhances per-

meation performance while compromising mechanical strength. And also, the membrane with high porosity and low tortuosity exhibits enhanced CO<sub>2</sub> flux; however, it is prone to molten carbonate runoff and hence poor stability of the membrane. Thus, the aggressive development of permeability may compromise the guaranteed mechanical strength and stability of the membrane. In the following paragraphs, we will conduct a comprehensive analysis and provide detailed explanations regarding the factors of materials, membrane thickness, and pore structure.

As we know, the CO<sub>2</sub> permeation flux can be directly enhanced by the development of internal factors, such as superior materials, thinner thickness, and a suitable pore structure (as mentioned above in Section 3.1). The selection of materials and thickness serves as a crucial prerequisite for the advancement of membrane technology. Indeed, for the ceramic-carbonate dual-phase membrane, we require a superior ceramic material with ultrahigh ionic conductivity to enhance the permeation flux, as the CO<sub>2</sub> permeation is dictated by the O<sup>2-</sup> conductivity within the ceramic support. Additionally, the mechanical strength of the material after membrane fabrication necessitates careful consideration. Thus, the integration of this field with the research domain of inorganic materials is essential for the exploration of novel materials, ultimately providing a wider array of options for membrane development. For instance, Ovalle-Encinia et al. fabricated a composite ceramic material derived from SDC and the perovskite Sm<sub>0.6</sub>Sr<sub>0.4</sub>Al<sub>0.3</sub>Fe<sub>0.7</sub>O<sub>3</sub>, which serves as a CO<sub>2</sub>/O<sub>2</sub> co-permeation membrane due to the presence of electron conductivity within the perovskite phase. The findings indicate that the carbonate membrane derived from this composite material exhibits superior permeability, selectivity, and mechanical strength in CO<sub>2</sub> separation at elevated temperatures (700–900 °C) [97]. The thickness of the membrane plays a crucial role in determining the permeation flux, with thinner membranes generally exhibiting an improvement in permeation capacity, which is a widely observed phenomenon in membrane separation processes. Thus, the implementation of appropriate techniques capable of efficiently reducing the membrane thickness should be incorporated during the preparation process.

In comparison to the aforementioned two terms, the optimization of the microstructure represents the future development direction for carbonate dual-phase systems. Precise control over the pore structure's ( $\epsilon$  and  $\tau$ ) parameters will result in significant enhancements to the CO<sub>2</sub> permeance of the membrane. Figure 15 illustrates the fundamental principle governing the pore structure. The configuration of the pore membrane, as demonstrated, exhibits a significant influence on the transport channels of CO<sub>3</sub><sup>2-</sup> ions. The big tortuosity within the membrane pore tends to markedly deflect the transport channels, whereas reduced tortuosity provides a relatively smooth path for the CO<sub>3</sub><sup>2-</sup> ions. Enhanced CO<sub>2</sub> permeance of the carbonate dual-phase membrane can be achieved through larger porosity and reduced tortuosity, as demonstrated in the aforementioned model (refer to Section 2). Nonetheless, indiscriminately pursuing a pore structure conducive to CO<sub>2</sub> permeation flux could potentially compromise the stability of the membrane system. The big porosity or small tortuosity will attenuate the capacity of the membrane support to retain molten carbonate. The molten carbonate is more prone to exiting the smooth carbonate channel of the membrane support, due to the influence of external forces such as gas pressure and gravity. The loss of carbonate directly results in the instability and degradation of CO<sub>2</sub> permeation. Therefore, a trade-off effect exists between the superior pore structure and membrane performance. For example, in the study of Zhang et al. [7], the SDC-carbonate dual-phase membrane fabricated using a "sacrificial template" technique exhibits superior pore structures in the SDC support. The value of the porosity ( $\epsilon$ ), tortuosity ( $\tau$ ), and ( $\epsilon/\tau$ ) are 0.531, 2.27, and 0.234, respectively, representing the most favorable pore structure to date. The CO<sub>2</sub> permeation flux has the potential to reach up to 1.84 mL·cm<sup>-2</sup>·min<sup>-1</sup> at 700 °C, despite the relatively thicker membrane thickness (1.5 mm). However, the CO<sub>2</sub> flux measured within this study demonstrates stability only for a duration of 10 to 15 h, as reported. The primary cause of the CO<sub>2</sub> flux degradation is directly attributable to the absence of the molten carbonate phase. The interplay between the pore structure of the

membrane and CO<sub>2</sub> permeation is instrumental in determining the long-term stability of the carbonate dual-phase membrane. Furthermore, an excessive level of porosity can render the membrane susceptible to fragility, thereby compromising its mechanical integrity. Thus, the interplay between the membrane structure and mechanical strength must be taken into account in the further development of membranes.

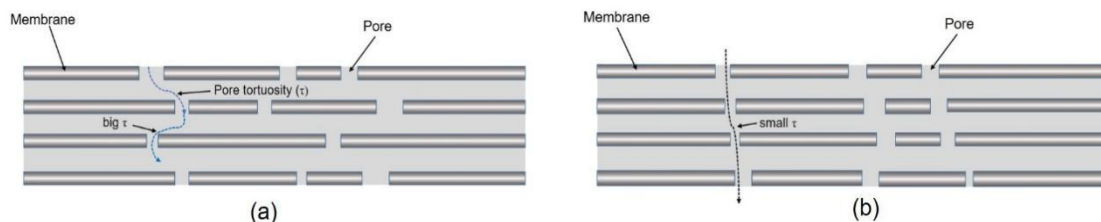


**Figure 15.** Visualization of the pore structure of the carbonate dual-phase membrane: (a) the big tortuosity within the membrane pore, (b) the membrane pore reduced tortuosity.

The current literature on carbonate dual-phase membrane reactors primarily investigates the coupling of a single reaction at one side of the membrane (refer to Figure 12). The novel membrane reactors, which couple different CO<sub>2</sub>-participant reactions at the feed and permeation sides, respectively, are also worth exploring in the future. The CO<sub>2</sub> generated from the feed side can undergo further conversion via the CO<sub>2</sub> reforming reaction at the permeation side. The propulsive force generated by the consumption reaction will exhibit greater intensity than that of the exclusive clearance of inert gas or vacuum treatment, a fact that has been corroborated numerous times in the realm of O<sup>2-</sup>-transport membrane reactors. Recent research by Wu et al. [98] has introduced a novel concept to enhance the developmental potential of the dual-phase membrane reactor. As shown in Figure 16, a dual-phase membrane fabricated from a perovskite support and carbonate phase enables CO<sub>2</sub>/O<sub>2</sub> counter-permeation under high-temperature conditions. In this model, CO<sub>2</sub> and O<sub>2</sub> are partitioned across the two sides of the membrane, rather than being presented on the same side. Thus, potential reactions, such as partial oxidation of hydrocarbons and autothermal methane reforming (AMR), can be investigated and integrated into a membrane reactor with CO<sub>2</sub>/O<sub>2</sub> counter permeation. For example, the occurrence of CO<sub>2</sub>-generated reactions is confined to one side of the membrane, with CO<sub>2</sub> subsequently permeating toward the opposing side. The oxygen required for partial oxidation reaction is supplied from the air feed side opposite the membrane, thereby eliminating the need for an additional air separation unit in this instance. Thus, the investigation of membrane reactors founded on carbonate dual-phase membranes represents a promising avenue for future research.

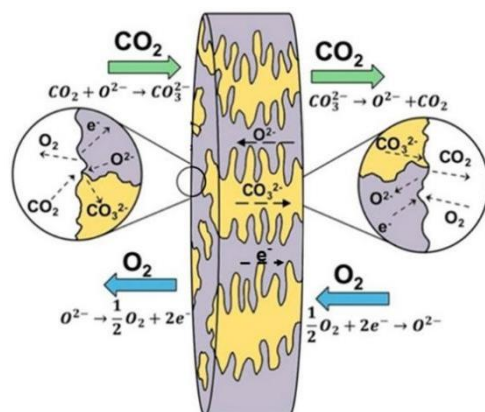


**Figure 16.** CO<sub>2</sub>/O<sub>2</sub> counter-permeation concept through a dense perovskite-carbonate dual-phase membrane (reprinted from [98] with permission of Elsevier).

### 6.3. Future Challenges

There is still a long way to go for the application of inorganic-carbonate dual-phase membranes in the industrial field. Inorganic-carbonate dual-phase membranes almost undergo three stages or aspects, as shown in Figure 17. Basically, the development processes include metal-carbonate membrane exploration, ceramic-carbonate membrane exploration, and membrane modification. Till now, the primary challenge faced by the membranes lies in achieving a balance between their permeability and stability. For the polymer or porous inorganic membranes, the permeability and selectivity generally have a trade-off effect. However, for the inorganic-carbonate dual-phase, this trade-off effect is reflected in permeability and stability. Regarding this challenge, the following four points need to be addressed in the future:

- (1) The continuous development of ceramic or metal materials exhibiting high  $O^{2-}$  or  $e^-$  conductance is imperative in order to enhance the permeability and mechanical strength of the inorganic-carbonate dual-phase membrane.
- (2) Improved preparation technologies should continue to be developed to fabricate homogeneously porous solid matrices with big porosity, small tortuosity, and uniformly distributed pores.
- (3) Surface modification of membrane support can be explored. This modification may improve surface reaction between the  $CO_2$  with support surface and molten carbonate phase. Additionally, this modification has the potential to enhance the interfacial wettability between the solid and carbonate phases, thereby reducing carbonate loss and ultimately improving membrane stability.
- (4) Modification of the molten carbonate is an unexplored area. This modification may increase the reaction rate of the triple-phase boundary (solid, molten carbonate, and gas molecular), and also increase the interfacial wettability between the solid and carbonate phases.

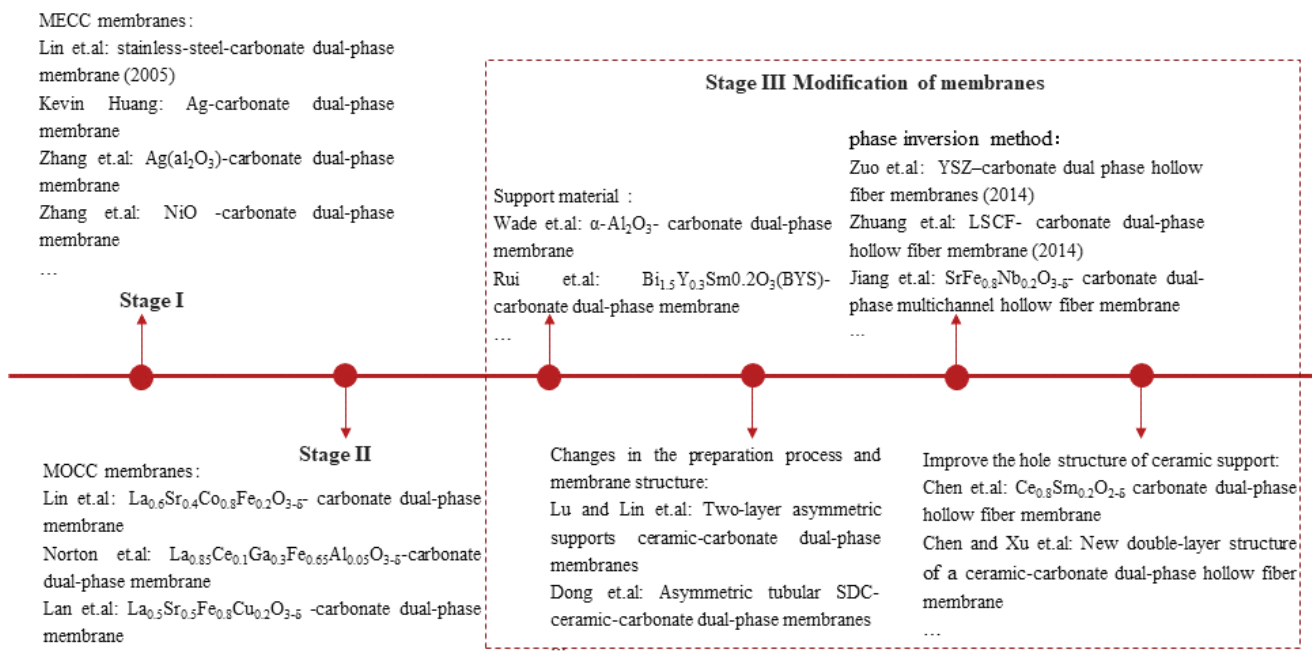


**Figure 17.** Three stages of an inorganic-carbonate dual-phase membrane. Lin, 2005 [14], Kevin Huang, 2012 [35], Zhang et al., 2014 [37], Zhang et al., 2017 [99], Lin et al., 2010 [6], Norton et al., 2010 [55], Lan et al., 2014 [42], Wade et al., 2011 [32], Rui et al., 2012 [44], Lu and Lin, 2013 [46], Dong et al., 2013 [27], Zuo et al., 2014 [48], Zhuang et al., 2014 [49], Jiang et al., 2016 [50], Chen et al., 2020 [51], Chen and Xu, 2022 [22].

## 7. Conclusions

Significant advancements have been made in comprehending the rationale and material development of the dense carbonate dual-phase membrane. The significant enhancement of CO<sub>2</sub> permeation properties and stability in the membrane has been observed in recent years. The novel membrane demonstrates significant advantages in the continuous capture of CO<sub>2</sub> at elevated temperatures, demonstrating potential for commercial development. However, certain complexities and challenges remain in the separation and reaction processes throughout the development cycle. The key challenges that need to be addressed in the improvement of carbonate dual-phase membranes and reactors include enhancing the packing density of membrane modules, further optimizing permeance levels, inefficient sealing at high temperature, and balance of the structure and mechanical strength of the membrane. Furthermore, a significant reduction in the cost of dual-phase membranes is required, which hinges on the expenses associated with raw materials, synthetic procedures, and membrane fabrication.

**Funding:** We are grateful to National Natural Science Foundation of China (Grant No. 22308168), Science and Technology Planning Project of Inner Mongolia Autonomous Region (Grant No. 2021GG0328), Natural Science Foundation of Inner Mongolia (Grant No. 2021BS02015), and Program for Young Talents of Science and Technology in Universities of Inner Mongolia Autonomous Region (Grant No. NJYT22086).

**Data Availability Statement:** Data availability is not applicable to this article as no new data were created or analyzed in this study.

**Conflicts of Interest:** Author Xuechao Hu was employed by the company Inner Mongolia Power (Group) Co., Ltd. The remaining authors declare that the research was conducted in the absence of any commercial or financial relationships that could be construed as a potential conflict of interest.

## References

1. Wang, Q.A.; Luo, J.Z.; Zhong, Z.Y.; Borgna, A. CO<sub>2</sub> capture by solid adsorbents and their applications: Current status and new trends. *Energy Environ. Sci.* **2011**, *4*, 42–55. [\[CrossRef\]](#)
2. Zhang, Y.G.; Chan, J.Y.G. Sustainable chemistry: Imidazolium salts in biomass conversion and CO<sub>2</sub> fixation. *Energy Environ. Sci.* **2010**, *3*, 408–417. [\[CrossRef\]](#)
3. Lin, J.Y.S. Molecular sieves for gas separation. *Science* **2016**, *353*, 121. [\[CrossRef\]](#) [\[PubMed\]](#)
4. Lin, Y.S. Inorganic Membranes for Process Intensification: Challenges and Perspective. *Ind. Eng. Chem. Res.* **2019**, *58*, 5787–5796. [\[CrossRef\]](#)
5. Shi, L.; Lai, L.S.; Tay, W.H.; Yeap, S.P.; Yeong, Y.F. Membrane Fabrication for Carbon Dioxide Separation: A Critical Review. *ChemBioEng Rev.* **2022**, *9*, 556–573. [\[CrossRef\]](#)
6. Anderson, M.; Lin, Y.S. Carbonate–ceramic dual-phase membrane for carbon dioxide separation. *J. Membr. Sci.* **2010**, *357*, 122–129. [\[CrossRef\]](#)
7. Zhang, L.; Xu, N.; Li, X.; Wang, S.; Huang, K.; Harris, W.H.; Chiu, W.K.S. High CO<sub>2</sub> permeation flux enabled by highly interconnected three-dimensional ionic channels in selective CO<sub>2</sub> separation membranes. *Energy Environ. Sci.* **2012**, *5*, 8310–8317. [\[CrossRef\]](#)
8. Miller, C.F.; Carolan, M.F.; Chen, C.M.; Minford, E.; Waldron, W.E.; Stepan, J.J. ITM ceramic membrane technology to produce synthesis gas. *J. Am. Chem. Soc.* **2007**, *234*.
9. Wei, Y.; Yang, W.; Caro, J.; Wang, H. Dense ceramic oxygen permeable membranes and catalytic membrane reactors. *Chem. Eng. J.* **2013**, *220*, 185–203. [\[CrossRef\]](#)
10. Way, J.D. *A Mechanistic Study of Chemically Modified Inorganic Membranes for Gas and Liquid Separations*; Colorado School of Mines: Golden, CO, USA, 2011.
11. Abdel-Salam, O.E.; Winnick, J. Simulation of an electrochemical carbon dioxide concentrator. *AIChE J.* **1976**, *22*, 1042–1050. [\[CrossRef\]](#)
12. Weaver, J.L.; Winnick, J. The molten carbonate carbon dioxide concentrator—Cathode performance at high CO<sub>2</sub> utilization. *J. Electrochem. Soc.* **1983**, *130*, 20–28. [\[CrossRef\]](#)
13. Kasai, H.; Matsuo, T.; Hosaka, M.; Motohira, N.; Ken-Ichiro, O.T.A. High temperature electrochemical separation of carbon dioxide using molten carbonate. *Denki Kagaku.* **1998**, *66*, 635–640. [\[CrossRef\]](#)
14. Chung, S.J.; Park, J.H.; Li, D.; Ida, J.I.; Kumakiri, I.; Lin, J.Y.S. Dual-Phase Metal–Carbonate Membrane for High-Temperature Carbon Dioxide Separation. *Ind. Eng. Chem. Res.* **2005**, *44*, 7999–8006. [\[CrossRef\]](#)
15. Rui, Z.B.; Anderson, M.; Lin, Y.S.; Li, Y.D. Modeling and analysis of carbon dioxide permeation through ceramic-carbonate dual-phase membranes. *J. Membr. Sci.* **2009**, *345*, 110–118. [\[CrossRef\]](#)

16. Rui, Z.; Ji, H.; Lin, Y.S. Modeling and analysis of ceramic–carbonate dual-phase membrane reactor for carbon dioxide reforming with methane. *Int. J. Hydrogen Energy* **2011**, *36*, 8292–8300. [[CrossRef](#)]
17. Tong, J.; Zhang, L.; Han, M.; Huang, K. Electrochemical separation of CO<sub>2</sub> from a simulated flue gas with high-temperature ceramic–carbonate membrane: New observations. *J. Membr. Sci.* **2015**, *477*, 1–6. [[CrossRef](#)]
18. Peng-Fei, C.; Bingrui, L.; Tao, H.; Kunyue, X.; Shiwang, C.; Panchao, Y.; Alexander, K.; Tomonori, S. Robust and Elastic Polymer Membranes with Tunable Properties for Gas Separation. *ACS Appl. Mater. Inter.* **2017**, *9*, 26483–26491.
19. Chiu, W.; Park, I.-S.; Shqau, K.; White, J.; Schillo, M.; Ho, W.; Dutta, P.; Verweij, H. Post-synthesis defect abatement of inorganic membranes for gas separation. *J. Membr. Sci.* **2011**, *377*, 182–190. [[CrossRef](#)]
20. Krishna, R.; van Baten, J.M.J.S.; Technology, P. A comparison of the CO<sub>2</sub> capture characteristics of zeolites and metal–organic frameworks. *Sep. Purif. Technol.* **2012**, *87*, 120–126. [[CrossRef](#)]
21. Dong, X.; Wu, H.-C.; Lin, Y.S. CO<sub>2</sub> permeation through asymmetric thin tubular ceramic-carbonate dual-phase membranes. *J. Membr. Sci.* **2018**, *564*, 73–81. [[CrossRef](#)]
22. Chen, T.; Xu, Y.; Zhang, Y.; Gong, Y.; Zhang, Y.; Lin, J.Y.S. Double-layer ceramic-carbonate hollow fiber membrane with superior mechanical strength for CO<sub>2</sub> separation. *J. Membr. Sci.* **2022**, *658*, 120701. [[CrossRef](#)]
23. Ortiz-Landeros, J.; Norton, T.; Lin, Y.S. Effects of support pore structure on carbon dioxide permeation of ceramic-carbonate dual-phase membranes. *Chem. Eng. Sci.* **2013**, *104*, 891–898. [[CrossRef](#)]
24. Norton, T.T.; Lu, B.; Lin, Y.S. Carbon dioxide permeation properties and stability of samarium-doped-ceria carbonate dual-phase membranes. *J. Membr. Sci.* **2014**, *467*, 244–252. [[CrossRef](#)]
25. Patricio, S.G.; Soares, C.M.C.; Santos, C.F.N.; Figueiredo, F.M.L.; Marques, F.M.B. Ceria-based substrates for CO<sub>2</sub> separation membranes. *Solid State Ionics* **2014**, *262*, 248–252. [[CrossRef](#)]
26. Patricio, S.G.; Papaioannou, E.I.; Ray, B.M.; Metcalfe, I.S.; Marques, F.M.B. Composite CO<sub>2</sub> separation membranes: Insights on kinetics and stability. *J. Membr. Sci.* **2017**, *541*, 253–261. [[CrossRef](#)]
27. Dong, X.; Ortiz Landeros, J.; Lin, Y.S. An asymmetric tubular ceramic-carbonate dual phase membrane for high temperature CO<sub>2</sub> separation. *Chem. Commun.* **2013**, *49*, 9654–9656. [[CrossRef](#)]
28. Baker, R.W. Future directions of membrane gas separation technology. *Ind. Eng. Chem. Res.* **2002**, *41*, 1393–1411. [[CrossRef](#)]
29. Baker, R.W.; Low, B.T. Gas Separation Membrane Materials: A Perspective. *Macromolecules.* **2014**, *47*, 6999–7013. [[CrossRef](#)]
30. Li, K. *Ceramic Membranes for Separation and Reaction*; John Wiley & Sons: West Sussex, UK, 2010; Volume 82, p. 554.
31. Gude, U.; Baumann, S.; Albert Meulenber, W.; Müller, M. Towards the development of materials for chemically stable carbonate-ceramic membranes to be used for CO<sub>2</sub> separation in water-gas-shift reactors. *Sep. Purif. Technol.* **2019**, *215*, 378–383. [[CrossRef](#)]
32. Wade, J.L.; Lee, C.; West, A.C.; Lackner, K.S. Composite electrolyte membranes for high temperature CO<sub>2</sub> separation. *J. Membr. Sci.* **2011**, *369*, 20–29. [[CrossRef](#)]
33. Li, D.F.; Wang, R.; Chung, T.S. Fabrication of lab-scale hollow fiber membrane modules with high packing density. *Sep. Purif. Technol.* **2004**, *40*, 15–30. [[CrossRef](#)]
34. Janz, G.J.; Tomkins, R. *Physical Properties Data Compilations Relevant to Energy Storage, 4: Molten Salts: Data on Additional Single and Multicomponent Salt Systems*; National Bureau of Standards: Washington, DC, USA, 1981; Volume 861.
35. Xu, N.; Li, X.; Franks, M.A.; Zhao, H.; Huang, K. Silver-molten carbonate composite as a new high-flux membrane for electrochemical separation of CO<sub>2</sub> from flue gas. *J. Membr. Sci.* **2012**, *401–402*, 190–194. [[CrossRef](#)]
36. Zhang, L.; Gong, Y.; Brinkman, K.S.; Wei, T.; Wang, S.; Huang, K. Flux of silver-carbonate membranes for post-combustion CO<sub>2</sub> capture: The effects of membrane thickness, gas concentration and time. *J. Membr. Sci.* **2014**, *455*, 162–167. [[CrossRef](#)]
37. Zhang, L.; Gong, Y.; Yaggie, J.; Wang, S.; Romito, K.; Huang, K. Surface modified silver-carbonate mixed conducting membranes for high flux CO<sub>2</sub> separation with enhanced stability. *J. Membr. Sci.* **2014**, *453*, 36–41. [[CrossRef](#)]
38. Zhang, L.; Tong, J.; Gong, Y.; Han, M.; Wang, S.; Huang, K. Fast electrochemical CO<sub>2</sub> transport through a dense metal-carbonate membrane: A new mechanistic insight. *J. Membr. Sci.* **2014**, *468*, 373–379. [[CrossRef](#)]
39. Tong, J.; Si, F.; Zhang, L.; Fang, J.; Huang, K. Stabilizing electrochemical carbon capture membrane with Al<sub>2</sub>O<sub>3</sub> thin-film overcoating synthesized by chemical vapor deposition. *Chem. Commun.* **2015**, *51*, 2936–2938. [[CrossRef](#)] [[PubMed](#)]
40. Fang, J.; Tong, J.; Huang, K. A superior mixed electron and carbonate-ion conducting metal-carbonate composite membrane for advanced flue-gas carbon capture. *J. Membr. Sci.* **2016**, *505*, 225–230. [[CrossRef](#)]
41. Norton, T.T.; Lin, Y.S. Ceramic–carbonate dual-phase membrane with improved chemical stability for carbon dioxide separation at high temperature. *Solid State Ion.* **2014**, *263*, 172–179. [[CrossRef](#)]
42. Lan, R.; Abdallah, S.M.M.; Amar, I.A.; Tao, S. Preparation of dense La<sub>0.5</sub>Sr<sub>0.5</sub>Fe<sub>0.8</sub>Cu<sub>0.2</sub>O<sub>3–δ</sub>–(Li,Na)<sub>2</sub>CO<sub>3</sub>–LiAlO<sub>2</sub> composite membrane for CO<sub>2</sub> separation. *J. Membr. Sci.* **2014**, *468*, 380–388. [[CrossRef](#)]
43. Li, Y.; Rui, Z.; Xia, C.; Anderson, M.; Lin, Y.S. Performance of ionic-conducting ceramic/carbonate composite material as solid oxide fuel cell electrolyte and CO<sub>2</sub> permeation membrane. *Catal. Today* **2009**, *148*, 303–309. [[CrossRef](#)]
44. Rui, Z.; Anderson, M.; Li, Y.; Lin, Y.S. Ionic conducting ceramic and carbonate dual phase membranes for carbon dioxide separation. *J. Membr. Sci.* **2012**, *417–418*, 174–182. [[CrossRef](#)]
45. Mori, T.; Wang, Y.; Drennan, J.; Auchterlonie, G.; Li, J.G.; Ikegami, T. Influence of particle morphology on nanostructural feature and conducting property in Sm-doped CeO<sub>2</sub> sintered body. *Solid State Ion.* **2004**, *175*, 641–649. [[CrossRef](#)]
46. Lu, B.; Lin, Y.S. Synthesis and characterization of thin ceramic-carbonate dual-phase membranes for carbon dioxide separation. *J. Membr. Sci.* **2013**, *444*, 402–411. [[CrossRef](#)]

47. Lu, B.; Lin, Y.S. Asymmetric Thin Samarium Doped Cerium Oxide–Carbonate Dual-Phase Membrane for Carbon Dioxide Separation. *Ind. Eng. Chem. Res.* **2014**, *53*, 13459–13466. [[CrossRef](#)]
48. Zuo, M.; Zhuang, S.; Tan, X.; Meng, B.; Yang, N.; Liu, S. Ionic conducting ceramic–carbonate dual phase hollow fibre membranes for high temperature carbon dioxide separation. *J. Membr. Sci.* **2014**, *458*, 58–65. [[CrossRef](#)]
49. Zhuang, S.; Li, Y.; Zuo, M.; Tan, X.; Meng, B.; Yang, N.; Liu, S. Dense composite electrolyte hollow fibre membranes for high temperature CO<sub>2</sub> separation. *Sep. Purif. Technol.* **2014**, *132*, 712–718. [[CrossRef](#)]
50. Jiang, X.; Zhu, J.; Liu, Z.; Guo, S.; Jin, W. CO<sub>2</sub>-Tolerant SrFe<sub>0.8</sub>Nb<sub>0.2</sub>O<sub>3-δ</sub>–Carbonate Dual-Phase Multichannel Hollow Fiber Membrane for CO<sub>2</sub> Capture. *Ind. Eng. Chem. Res.* **2016**, *55*, 3300–3307. [[CrossRef](#)]
51. Chen, T.; Wang, Z.; Hu, J.; Wai, M.H.; Lin, Y.S. High CO<sub>2</sub> permeability of ceramic-carbonate dual-phase hollow fiber membrane at medium-high temperature. *J. Membr. Sci.* **2020**, *597*, 117770. [[CrossRef](#)]
52. Zeng, S.; Liu, Z.; Zhao, H.; Yang, T.; Dong, X.; Du, Z.J.S.; Technology, P. A chemically stable La<sub>0.2</sub>Sr<sub>0.8</sub>Fe<sub>0.9</sub>Mo<sub>0.1</sub>O<sub>3-δ</sub>-molten carbonate dual-phase membrane for CO<sub>2</sub> separation. *Sep. Purif. Technol.* **2022**, *280*, 119970. [[CrossRef](#)]
53. Wang, S.; Tong, J.; Cui, L.; Zhang, P.; Zhou, F. A layered perovskite La<sub>1.5</sub>Sr<sub>0.5</sub>NiO<sub>4+δ</sub>-molten carbonate dual-phase membrane for CO<sub>2</sub> capture from simulated flue gas. *J. Membr. Sci.* **2022**, *647*, 120278. [[CrossRef](#)]
54. Kazakli, M.; Mutch, G.A.; Triantafyllou, G.; Gil, A.G.; Li, T.; Wang, B.; Bailey, J.J.; Brett, D.J.; Shearing, P.R.; Li, K.; et al. Controlling molten carbonate distribution in dual-phase molten salt-ceramic membranes to increase carbon dioxide permeation rates. *J. Membr. Sci.* **2021**, *617*, 118640. [[CrossRef](#)]
55. Norton, T.T.; Ortiz-Landeros, J.; Lin, Y.S. Stability of La–Sr–Co–Fe Oxide–Carbonate Dual-Phase Membranes for Carbon Dioxide Separation at High Temperatures. *Ind. Eng. Chem. Res.* **2014**, *53*, 2432–2440. [[CrossRef](#)]
56. Yan, A.; Cheng, M.; Dong, Y.; Yang, W.; Maragou, V.; Song, S.; Tsiakaras, P. Investigation of a Ba<sub>0.5</sub>Sr<sub>0.5</sub>Co<sub>0.8</sub>Fe<sub>0.2</sub>O<sub>3-δ</sub> based cathode IT-SOFC—I. The effect of CO<sub>2</sub> on the cell performance. *Appl. Catal. B* **2006**, *66*, 64–71. [[CrossRef](#)]
57. Yi, J.; Feng, S.; Zuo, Y.; Liu, W.; Chen, C. Oxygen Permeability and Stability of Sr<sub>0.95</sub>Co<sub>0.8</sub>Fe<sub>0.2</sub>O<sub>3-δ</sub> in a CO<sub>2</sub>- and H<sub>2</sub>O-Containing Atmosphere. *J. Cheminformatics* **2005**, *17*, 5856–5861. [[CrossRef](#)]
58. Sun, S.; Wen, Y.; Huang, K. A New Ceramic–Carbonate Dual-Phase Membrane for High-Flux CO<sub>2</sub> Capture. *ACS Sustain. Chem. Eng.* **2021**, *9*, 5454–5460. [[CrossRef](#)]
59. Chen, T.; Yu, B.; Zhao, Y.; Li, Y.; Lin, Y.S. Carbon Dioxide Permeation through Ceramic-carbonate Dual-Phase Membrane—Effects of Sulfur Dioxide. *J. Membr. Sci.* **2017**, *540*, 477–484. [[CrossRef](#)]
60. Chen, T.J.; Wu, H.C.; Li, Y.D.; Lin, Y.S. Poisoning Effect of H<sub>2</sub>S on CO<sub>2</sub> Permeation of Samarium-Doped-Ceria/Carbonate Dual-Phase Membrane. *Ind. Eng. Chem. Res.* **2017**, *56*, 14662–14669. [[CrossRef](#)]
61. Wei, Y.; Ravkina, O.; Klande, T.; Wang, H.; Feldhoff, A. Effect of CO<sub>2</sub> and SO<sub>2</sub> on oxygen permeation and microstructure of Pr<sub>0.9</sub>La<sub>0.12</sub>Ni<sub>0.74</sub>Cu<sub>0.21</sub>Ga<sub>0.05</sub>O<sub>4+δ</sub> membranes. *J. Membr. Sci.* **2013**, *429*, 147–154. [[CrossRef](#)]
62. Gao, J.; Li, L.; Yin, Z.; Zhang, J.; Lu, S.; Tan, X. Poisoning effect of SO<sub>2</sub> on the oxygen permeation behavior of La<sub>0.6</sub>Sr<sub>0.4</sub>Co<sub>0.2</sub>Fe<sub>0.8</sub>O<sub>3-δ</sub> perovskite hollow fiber membranes. *J. Membr. Sci.* **2014**, *455*, 341–348. [[CrossRef](#)]
63. Mohn, H.; Wendt, H. Molecular Thermodynamics of Molten Salt Evaporation. *Ztschrift Für Physikalische Chemie* **1995**, *192*, 101–119. [[CrossRef](#)]
64. Xing, W.; Peters, T.; Fontaine, M.-L.; Evans, A.; Henriksen, P.P.; Norby, T.; Bredesen, R. Steam-promoted CO<sub>2</sub> flux in dual-phase CO<sub>2</sub> separation membranes. *J. Membr. Sci.* **2015**, *482*, 115–119. [[CrossRef](#)]
65. Xing, W.; Li, Z.; Peters, T.; Fontaine, M.-L.; McCann, M.; Evans, A.; Norby, T.; Bredesen, R. Improved CO<sub>2</sub> flux by dissolution of oxide ions into the molten carbonate phase of dual-phase CO<sub>2</sub> separation membranes. *Sep. Purif.* **2019**, *212*, 721–727. [[CrossRef](#)]
66. Gili, A.; Bischoff, B.; Simon, U.; Schmidt, F.; Kober, D.; Görke, O.; Bekheet, M.F.; Gurlo, A. Ceria-Based Dual-Phase Membranes for High-Temperature Carbon Dioxide Separation: Effect of Iron Doping and Pore Generation with MgO Template. *Membranes* **2019**, *9*, 108. [[CrossRef](#)] [[PubMed](#)]
67. Zhang, P.; Wang, S.; Pang, B.; Zhu, X.; Yang, W. Effect of molten carbonate composition on CO<sub>2</sub> permeation mechanism. *J. Membr. Sci.* **2022**, *645*, 120210. [[CrossRef](#)]
68. Chen, T.; Wang, Z.; Das, S.; Liu, L.; Li, Y.; Kawi, S.; Lin, Y.S. A novel study of sulfur-resistance for CO<sub>2</sub> separation through asymmetric ceramic-carbonate dual-phase membrane at high temperature. *J. Membr. Sci.* **2019**, *581*, 72–81. [[CrossRef](#)]
69. Kathiraser, Y.; Wang, Z.; Yang, N.-T.; Zahid, S.; Kawi, S. Oxygen permeation and stability study of La<sub>0.6</sub>Sr<sub>0.4</sub>Co<sub>0.8</sub>Ga<sub>0.2</sub>O<sub>3-δ</sub> (LSCG) hollow fiber membrane with exposure to CO<sub>2</sub>, CH<sub>4</sub> and He. *J. Membr. Sci.* **2013**, *427*, 240–249. [[CrossRef](#)]
70. Wang, Z.; Kathiraser, Y.; Kawi, S. High performance oxygen permeable membranes with Nb-doped BaBi<sub>0.05</sub>Co<sub>0.95</sub>O<sub>3-δ</sub> perovskite oxides. *J. Membr. Sci.* **2013**, *431*, 180–186. [[CrossRef](#)]
71. Yang, N.T.; Kathiraser, Y.; Kawi, S. A new asymmetric SrCo<sub>0.8</sub>Fe<sub>0.1</sub>Ga<sub>0.1</sub>O<sub>3-δ</sub> perovskite hollow fiber membrane for stable oxygen permeability under reducing condition. *J. Membr. Sci.* **2013**, *428*, 78–85. [[CrossRef](#)]
72. Anantharaman, R.; Peters, T.; Xing, W.; Fontaine, M.L.; Bredesen, R. Dual phase high-temperature membranes for CO<sub>2</sub> separation—performance assessment in post- and pre-combustion processes. *Faraday Discuss.* **2016**, *192*, 251–269. [[CrossRef](#)]
73. Xu, X.; Song, C.; Wincek, R.; Andresen, J.; Miller, B.; Scaroni, A. Separation of CO<sub>2</sub> from Power Plant Flue Gas Using a Novel CO<sub>2</sub> "Molecular Basket" Adsorbent. *Fuel Chem. Div. Prepr.* **2003**, *48*, 162–163.
74. Samanta, A.; Zhao, A.; Shimizu, G.K.H.; Sarkar, P.; Gupta, R. Post-Combustion CO<sub>2</sub> Capture Using Solid Sorbents: A Review. *Ind. Eng. Chem. Res.* **2012**, *51*, 1438–1463. [[CrossRef](#)]

75. Scholes, C.A.; Smith, K.H.; Kentish, S.E.; Stevens, G.W. CO<sub>2</sub> capture from pre-combustion processes—Strategies for membrane gas separation. *Int. J. Greenh. Gas Control* **2010**, *4*, 739–755. [[CrossRef](#)]
76. Ku, A.Y.; Kulkarni, P.; Shisler, R.; Wei, W. Membrane performance requirements for carbon dioxide capture using hydrogen-selective membranes in integrated gasification combined cycle (IGCC) power plants. *J. Membr. Sci.* **2011**, *367*, 233–239. [[CrossRef](#)]
77. Anderson, M.; Lin, Y.S. Carbon dioxide separation and dry reforming of methane for synthesis of syngas by a dual-phase membrane reactor. *AIChE J.* **2013**, *59*, 2207–2218. [[CrossRef](#)]
78. Berstad, D.; Neke, P.; Anantharaman, R. Low-temperature CO<sub>2</sub> Removal from Natural Gas. *Energy Procedia* **2012**, *26*, 41–48. [[CrossRef](#)]
79. Maas, P.; Scherer, V. Lignite Fired IGCC With Ceramic Membranes for CO<sub>2</sub> Separation. *Energy Procedia* **2014**, *63*, 1976–1985. [[CrossRef](#)]
80. Zhang, P.; Tong, J.; Huang, K. Combining Electrochemical CO<sub>2</sub> Capture with Catalytic Dry Methane Reforming in a Single Reactor for Low-Cost Syngas Production. *ACS Sustain. Chem. Eng.* **2016**, *4*, 7056–7065. [[CrossRef](#)]
81. Zhang, P.; Tong, J.; Huang, K. Dry-Oxy Methane Reforming with Mixed e<sup>-</sup>/CO<sub>3</sub><sup>2-</sup> Conducting Membranes. *ACS Sustain. Chem. Eng.* **2017**, *5*, 5432–5439. [[CrossRef](#)]
82. Zhang, P.; Tong, J.; Huang, K. Self-Formed, Mixed-Conducting, Triple-Phase Membrane for Efficient CO<sub>2</sub>/O<sub>2</sub> Capture from Flue Gas and in Situ Dry-Oxy Methane Reforming. *ACS Sustain. Chem. Eng.* **2018**, *6*, 14162–14169. [[CrossRef](#)]
83. Chen, T.; Wang, Z.; Liu, L.; Pati, S.; Kawi, S. Coupling CO<sub>2</sub> separation with catalytic reverse water-gas shift reaction via ceramic-carbonate dual-phase membrane reactor. *Chem. Eng. J.* **2020**, *379*, 122182. [[CrossRef](#)]
84. Pang, B.; Zhang, P.; Cao, Z.; Wang, S.; Tong, J.; Zhu, X.; Yang, W. Mixed oxygen ionic-carbonate ionic conductor membrane reactor for coupling CO<sub>2</sub> capture with in situ methanation. *AIChE J.* **2023**, *69*, 17919. [[CrossRef](#)]
85. Dong, X.; Lin, Y.S. Catalyst-free ceramic-carbonate dual phase membrane reactor for hydrogen production from gasifier syngas. *J. Membr. Sci.* **2016**, *520*, 907–913. [[CrossRef](#)]
86. Wu, H.-C.; Rui, Z.; Lin, J.Y.S. Hydrogen production with carbon dioxide capture by dual-phase ceramic-carbonate membrane reactor via steam reforming of methane. *J. Membr. Sci.* **2020**, *598*, 117780. [[CrossRef](#)]
87. Wang, Z.; Kathiraser, Y.; Soh, T.; Kawi, S. Ultra-high oxygen permeable BaBiCoNb hollow fiber membranes and their stability under pure CH<sub>4</sub> atmosphere. *J. Membr. Sci.* **2014**, *465*, 151–158. [[CrossRef](#)]
88. Zhu, J.; Dong, Z.; Liu, Z.; Zhang, K.; Zhang, G.; Jin, W. Multichannel mixed-conducting hollow fiber membranes for oxygen separation. *AIChE J.* **2014**, *60*, 1969–1976. [[CrossRef](#)]
89. Wang, T.; Liu, Z.; Xu, X.; Zhu, J.; Jin, W. Insights into the design of nineteen-channel perovskite hollow fiber membrane and its oxygen transportation behaviour. *J. Membr. Sci.* **2020**, *595*, 117600. [[CrossRef](#)]
90. Caro, J.; Caspary, K.J.; Hamel, C.; Hoting, B.; Kölsch, P.; Langanke, B.; Nassauer, K.; Schiestel, T.; Schmidt, A.; Schomäcker, R.; et al. Catalytic Membrane Reactors for Partial Oxidation Using Perovskite Hollow Fiber Membranes and for Partial Hydrogenation Using a Catalytic Membrane Contactor. *Ind. Eng. Chem. Res.* **2007**, *46*, 2286–2294. [[CrossRef](#)]
91. Dong, X.; Zhang, C.; Chang, X.; Jin, W.; Xu, N. A self-catalytic membrane reactor based on a supported mixed-conducting membrane. *AIChE J.* **2008**, *54*, 1678–1680. [[CrossRef](#)]
92. Wang, H.; Feldhoff, A.; Caro, J.; Schiestel, T.; Werth, S. Oxygen selective ceramic hollow fiber membranes for partial oxidation of methane. *AIChE J.* **2010**, *55*, 2657–2664. [[CrossRef](#)]
93. Zeng, Y.; Lin, Y.S. Oxygen Permeation and Oxidative Coupling of Methane in Yttria Doped Bismuth Oxide Membrane Reactor. *J. Catal.* **2000**, *193*, 58–64. [[CrossRef](#)]
94. Akin, F.T.; Lin, Y.S.; Zeng, Y. Comparative Study on Oxygen Permeation and Oxidative Coupling of Methane on Disk-Shaped and Tubular Dense Ceramic Membrane Reactors. *Ind. Eng. Chem. Res.* **2001**, *40*, 5908–5916. [[CrossRef](#)]
95. Qi, X.; Akin, F.T.; Lin, Y.S. Ceramic-glass composite high temperature seals for dense ionic-conducting ceramic membranes. *J. Membr. Sci.* **2015**, *193*, 185–193. [[CrossRef](#)]
96. Di Felice, L.; Middelkoop, V.; Anzoletti, V.; Snijkers, F.; Annaland, M.; Gallucci, F. New high temperature sealing technique and permeability data for hollow fiber BSCF perovskite membranes. *Chem. Eng. Process.* **2016**, *107*, 206–219. [[CrossRef](#)]
97. Ovalle-Encinia, O.; Pfeiffer, H.; Ortiz-Landeros, J. Ce<sub>0.85</sub>Sm<sub>0.15</sub>O<sub>2</sub>-Sm<sub>0.6</sub>Sr<sub>0.4</sub>Al<sub>0.3</sub>Fe<sub>0.7</sub>O<sub>3</sub> composite for the preparation of dense ceramic-carbonate membranes for CO<sub>2</sub> separation. *J. Membr. Sci.* **2018**, *547*, 11–18. [[CrossRef](#)]
98. Wu, H.C.; Nile, G.; Lin, J.Y.S. Mixed-conducting ceramic-carbonate dual-phase membranes: Gas permeation and counter-permeation. *J. Membr. Sci.* **2020**, *605*, 118093. [[CrossRef](#)]
99. Zhang, P.; Tong, J.; Huang, K. A self-forming dual-phase membrane for high-temperature electrochemical CO<sub>2</sub> capture. *J. Mater.* **2017**, *5*, 12769–12773. [[CrossRef](#)]

**Disclaimer/Publisher’s Note:** The statements, opinions and data contained in all publications are solely those of the individual author(s) and contributor(s) and not of MDPI and/or the editor(s). MDPI and/or the editor(s) disclaim responsibility for any injury to people or property resulting from any ideas, methods, instructions or products referred to in the content.